CHARLES UNIVERSITY

FACULTY OF PHARMACY IN HRADEC KRÁLOVÉ

Department of Pharmaceutical Technology

Diploma thesis

Calcium phosphate bone cements: Synthesis, characterization and drug release properties

Jiří Doubek

Hradec Králové 2020

Supervisor: Dr. Georgios Paraskevopoulos, Ph.D.

I declare that this thesis is my original copyrighted work. All literature and other resources I used while processing are listed in the bibliography and properly cited. The thesis was not misused for obtaining the same or different academic degree.

In Hradec Králové 14. 5. 2020 Jiří Doubek

Acknowledgements

I would like to express my acknowledgement to Dr. Georgios Paraskevopoulos, Ph.D. who helped me with the transition of an Erasmus+ project to a diploma thesis. I am thankful for his advice and time, he invested in the corrections.

My special thanks go to Dr. Nikolaos Bouropoulos, Ph.D. who accepted me in his laboratory for an Erasmus+ project internship and who patiently introduced me to the area of material science. Furthermore, my gratitude goes to Emmanouela Mystiridou, Ph.D. and Elleni Anna Oikonomou who helped me with the operation of the laboratory equipment and were very supportive throughout my internship.

Lastly, I would like to thank Doc. PharmDr. Přemysl Mladěnka, Ph.D. and Erasmus+ project in general for allowing me to execute my research internship in Patra, Greece.

Contents

Abstrakt

Univerzita Karlova, Farmaceutická fakulta v Hradci Králové

Katedra farmaceutické technologie

Autor: Jiří Doubek

Školitel: Dr. Georgios Paraskevopoulos, Ph.D.

Název diplomové práce: Kostní cementy na bázi fosforečnanu vápenatého: Syntéza, charakterizace a uvlňování léčivé látky

Nesrůstající traumata kostí se v současnosti stávají komplikací, která je s to vyřadit pacienta z aktivního života po značnou dobu. Jelikož se kostní hmota skládá především z hydroxyapatitu, derivát fosforečnanu vápenatého - cement na bázi fosforečnanu vápenátého - je studován jako injekčně aplikovatelná kostní substituce. Vlastnosti takového cementu (injektabilita, bioaktivita a resorbovatelnost) se zdají být velmi slibné. Mimo to možnost podpořit proces hojení inkorporováním léčiva do formulace otevírá nové terapeutické možnosti. Cílem této práce bylo nejprve syntetizovat α-fosforečnan vápenatý vysoké kvality a charakterizovat jeho vlastnosti. Dále bylo cílem použít připravený α-fosforečnan vápenatý k přípravě injektabilní cementové pasty odolné vůči vymývání. Vlastnosti čistého i ibuprofenem obohaceného cementu byly zkoumány rentgenovou difrakcí, Ramanovou spektroskopií, měřením pevnosti v tlaku, skenovací elektronovou mikroskopií a disolucí.

Získaná data odhalila vysokou kvalitu izolovaného α-fosforečnanu vápenatého. Dále že většina α-fosforečnanu vápenatého je přeměněna v hydroxyapatit s nižším obsahem vápníku už po jednom dni tvrdnutí, zatímco stopy α-fosforečnanu vápenatého jsou patrné až do 15 dní tvrdnutí. Mimo to byl pozorován významný rozdíl mezi pevností v tlaku u čistého a ibuprofenem obohaceného cementu. Na druhou stranu obohacení ibuprofenem nemělo vliv na krystalickou strukturu cementu ani na hydratační reakci. Uvolňování ibuprofenu trvalo déle než 21 dní (kdy bylo dosaženo 80 % uvolněné látky) a řídilo se Higuchiho zákonem. Nakonec i injektabilita a odolnost vůči vymývání byly optimální. Experimentální výsledky naznačují, že cement na bázi fosforečnanu vápenatého by mohl být slibným nosičem léčiv.

Abstract

Charles University, Faculty of Pharmacy in Hradec Králové
Department of Pharmaceutical Technology
Author: Jiří Doubek
Supervisor: Dr. Georgios Paraskevopoulos, Ph.D.
Title of Thesis: Calcium phosphate bone cements: Synthesis, characterization and drug release properties

Non-healing bone traumas are currently a complication, which may disable a patient from active life for a long period. Due to the fact that bone mass consists mostly of hydroxyapatite, a derivative of calcium phosphate - calcium phosphate cement (CPC) - is studied as an injectable bone substitute. The cement's characteristics (low setting temperature, injectability, bioactivity, and resorbability) are very promising. Furthermore, the possibility to incorporate a drug in the formulation that would support the healing process opens a way for new therapeutic options. Firstly, the aim of this research was to synthesize a high-quality α-tricalcium phosphate (α-TCP) and characterize its properties. Subsequently, the prepared α-TCP was used for the preparation of an injectable and washout resistant cement paste. Finally, the properties of developed pure or ibuprofen-loaded cement were examined by X-ray diffraction, Raman spectra, compressive strength, scanning electron microscopy, and dissolution studies.

The obtained data revealed that α-TCP of high-quality was isolated. Furthermore, the majority of α-TCP to calcium-deficient hydroxyapatite conversion was completed after one day of hardening, while residues of α-TCP remained present even after 15 days. In addition, a significant difference between the compressive strength of pure CPC and ibuprofen-loaded CPC was noticed. Results also revealed that the drug incorporation did not affect the crystalline structure of CPC or the hydration reaction. The ibuprofen release lasted more than 21 days (reaching 80 % of the initial amount) and followed Higuchi's law. Finally, the injectability, as well as the washout resistance, were optimal. In conclusion, the experimental results suggest that the CPC might be a promising drug carrier.

1. Introduction and aim of the work

All bones and teeth of the human body are mainly composed of one constituent – calcium-deficient hydroxyapatite, which is a calcium phosphate derivative (1). The development of medicine in the postmodern world allows humans to live longer than ever before. Thus, a new need for materials that would substitute the bone tissue after traumas, especially in osteoporotic patients, emerges. Towards this direction, calcium phosphate bone cements have proved to be promising materials. They have been documented as early as 1832 by Ostermann but they have been initially studied by Chow and Brown (2). After that, a lot of research has been conducted on the field starting from allogenic bone transplants and later to polymeric grafts. The recent research expansion of calcium phosphate blocks proves that the future belongs to biodegradable materials in which small molecules or peptide drugs can be incorporated.

The aim of this work is to initially illustrate the role of calcium phosphate cements and highlight their structure and properties. For sake of comprehensiveness, a summary of natural bone healing and the properties of CPCs' predecessor, PMMA cement, are presented. In the practical part, the aim was the synthesis of calcium phosphate cement from commercially available raw materials. After quality control, an effort to prepare injectable and washout resistant cement paste took place. The obtained cement was studied during the process of hardening and the drug release properties of ibuprofen loaded cement were examined.

2. List of Abbreviations

α-TCP	α-tricalcium phosphate
β-TCP	β-tricalcium phosphate
BMP	bone morphogenic protein
Ca/P	calcium/phosphate
CaP	calcium phosphate
CPC	calcium phosphate cement
DCPD	dicalcium phosphate dihydrate
EMA	European medicines agency
EU	European Union
FDA	food and drug administration
FGF	fibroblast growth factor
HPLC	high-performance liquid chromatography
JP	Japanese pharmacopoeia
M-CSF	macrophage-colony stimulating factor
OPG	osteoprotegerin
PBS	phosphate buffer saline
Ph. Eur.	European pharmacopoeia
PMMA	polymethylmethacrylate
RANKL	receptor activator of nuclear factor kappa B
RPM	revolutions per minute
SEM	scanning electron microscopy
TeCP	tetracalcium phosphate
TGF-β	transforming growth factor β
TNF-α	tumor necrosis factor α
USP	United States pharmacopeia
UV/VIS	ultraviolet/visible light
VEGF	vascular endothelial growth factor
XRD	X-ray diffraction

3. Theoretical Part

3.1 Calcium phosphates

The term “calcium phosphates” is used to characterize a group of various compounds that contain calcium in their cationic part and phosphate in their anionic part. The anionic part can be hydrogenphosphate, dihydrogenphosphate, diphosphate, or triphosphate. It can also sometimes incorporate hydroxide, fluoride, chloride, etc. The use of calcium phosphates varies from crop fertilizers to feed-additives and toothpaste additives. Halophosphates are used as luminescent agents (3). In the research towards new bone substitutes, more derivatives of calcium phosphate emerge. However, all of them come from a family of orthophosphates (PO_4^{3-}) because pyrophosphates and metaphosphates tend to hydrolyze under physiological conditions. Moreover, the later found to cause extraosseous calcification (4). Calcium phosphates may differ in their chemical formula and thus in Ca/P ratio. In addition, they have different solubility, biodegradability, and synthesis conditions i.e. particularly whether they are precipitated from aqueous solutions (e.g., low-temperature CaP) or they are synthesized at high temperature (e.g., high-temperature CaP). Further examples of low-temperature calcium phosphates are monocalcium phosphate monohydrate, dicalcium phosphate, or precipitated hydroxyapatite. Typical representators of high-temperature calcium phosphates are α-tricalcium phosphate, β-tricalcium phosphate, or monocalcium phosphate (5).

3.1.1 Tricalcium phosphate

Calcium phosphate, tricalcium phosphate, or by IUPAC name tricalcium;diphosphate is an odorless white solid (6), practically insoluble in water, which is forming three crystalline forms: α-tricalcium phosphate, β-tricalcium phosphate, and α'-tricalcium phosphate. The thermodynamic stability corresponds to the theoretical density which is following the order: β-TCP>α-TCP>α'-TCP (see Figure 1) (7).

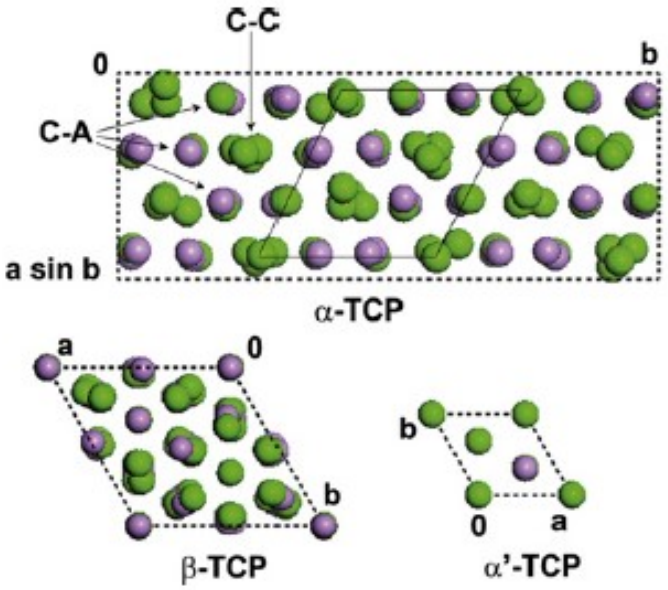

Figure 1: Crystalline structure of α-TCP, β-TCP, and α'-TCP. Ca^{2+}: green, P^{5+}: violet, O^{2-} is not represented. Solid rhombus in a-TCP relates to hydroxyapatite. Taken from Carrodeguas et al. (7).

3.1.1.1 α-tricalcium phosphate

Tricalcium phosphate is capable of forming three crystalline structures, from which only α-TCP and β-TCP are scientifically relevant because α'-TCP converts to α-TCP almost immediately (7). α-TCP is a metastable polymorph of tricalcium phosphate which is stable at temperatures higher than 1125 °C (8). If the α-TCP is exposed to a gradual drop in temperature, its crystalline structure changes in favor of the more stable polymorph – β-TCP. To prevent this shift, a sudden quenching from a very high temperature to room temperature must take place.

α-TCP crystallizes in a monoclinic crystal system. The more loosely packed structure, in contrast to that of β-TCP, increases the water solubility (7).

The synthesis of α-TCP from commercially available reagents is most often performed as described in Equation 1.

$$CaCO_{3\,(s)} + Ca_2P_2O_{7(s)} \xrightarrow{1450\ ^oC} Ca_3(PO_4)_{2(s)} + CO_2(g) \quad [1]$$

Equation 1: Synthesis of a-TCP

3.1.1.2 β-tricalcium phosphate

β-TCP is the only stable crystalline form of tricalcium phosphate at room temperature. Itcan be transformed to α-TCP by exposure to temperatures higher than 1125 °C. On the contrary, exposure of α-TCP to a gradual decrease of temperature from 1125 °C to room temperature, causes a change in crystalline structure to β-TCP. β-TCP crystalizes in rhombohedral crystal symmetry. The distinguishment between α and β polymorphs is performed by X-ray diffractometry. The most stable polymorph of tricalcium phosphate finds application in medicine and more specifically in the preparation of preset blocks or granules which are used as bone substitutes. (7).

3.1.2 Hydroxyapatite

Precipitated hydroxyapatite is the final product of all calcium phosphate cements when the reaction is taking place at pH > 4,2. On the other hand, for reactions set at pH < 4,2 the main product is the least soluble brushite (9).

Precipitated hydroxyapatite has a Ca/P molar ratio between 1,5-1,67 where 1,67 is the value of stoichiometric hydroxyapatite. Hydroxyapatite which is present in human bone tissue is rarely stoichiometric and the values of the Ca/P ratio are lower. High temperature synthesized hydroxyapatite can have a fixed molar Ca/P ratio of 1,67. Thus, hydroxyapatite present in bone tissue is often called calcium-deficient hydroxyapatite (10).

The crystalline structure of precipitated hydroxyapatite is very similar to the crystalline structure of α-TCP. This is visible in the previously shown Figure 1, where the crystal of hydroxyapatite is stressed out by solid line rhombus in the structure of α-TCP. The hydroxyl group of hydroxyapatite would appear in place of C-C (cation-cation) columns (7).

The degree of conversion from α-TCP to precipitated hydroxyapatite linearly correlates with the compressive strength of the final cement. Because of this, precipitated

hydroxyapatite or calcium-deficient hydroxyapatite is responsible for the mechanical properties of cement (11).

3.2 Natural bone cement

3.2.1 Natural bone constitution

Bones are the main structural support of the vertebral body while also having multiple functions e.g., calcium and phosphorus reservoir, mechanical protection of soft tissues, and site of blood formation.

Bones in the human body are divided into three categories: long bones, small bones, and flat bones. These categories have a different role in the organism and a different morphological structure. Long bones comprise a thick layer of compact bone in diaphysis covering the medullary cavity. Trabecular-spongy bone can be found in epiphysis and metaphysis. The function of long bones is to ease locomotion and support body mass. Small bones, on the other hand, comprise a thinner layer of compact bone with a denser net of a trabecular bone inside. Short bones provide support during movement in joints like an ankle or wrist. Flat bones consist of two compact bone layers with a small proportion of trabecular bone in between. Their prime role is to protect internal organs. Irregular bones are mainly vertebrae and pelvic bones that also protect vital organs. Sesamoid bones are anchored in tendons and thus support their function in joints (12).

Human bones are composed of organic and inorganic parts. The organic part consists of living cells – osteoblasts, osteoclasts, and osteocytes that form cca 5 % of the bone volume. The rest of the organic part is formed of collagen tissue with a small portion of proteoglycans and glycosaminoglycans forming the intercellular matrix. Type I collagen is produced by osteoblasts throughout the bone mass. One osteoblast produces approximately 1-2 μm^3 per day. When the collagen layer reaches 20 µm the deposition of calcium-deficient hydroxyapatite initiates (13).

The inorganic part of bone mass, which represents up to 50 % of bone volume, consists mainly of calcium-deficient hydroxyapatite. Calcium-deficient hydroxyapatite crystals occur in places between tropocollagen fibers. Thus, lamellar bone (Substantia compacta), which has a denser structure has also a higher proportion of calcium-deficient hydroxyapatite than trabecular bone (Substantia spongiosa), which is noticeably more porous (12). The detailed bone structure is depicted in Figure 2.

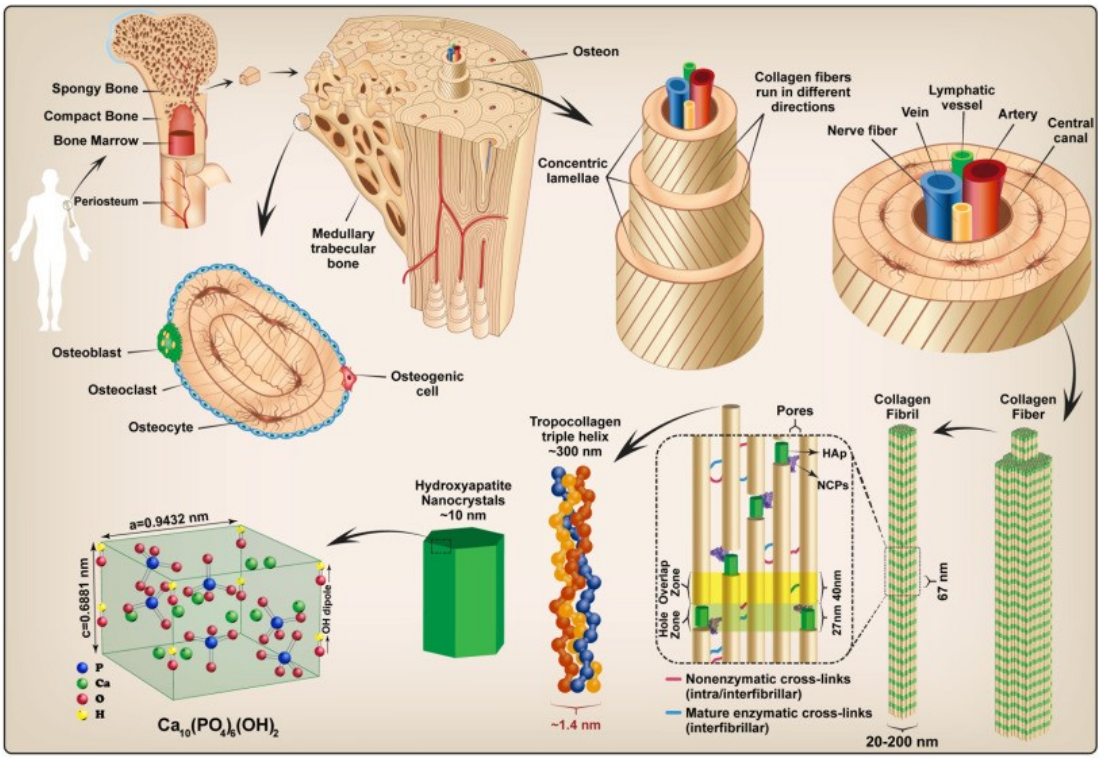

Figure 2: Macro-, micro-, and nanostructure of bone. Taken from Farokhi et al. (14).

In addition, the higher content of non-mineralized collagen in the trabecular bone makes it more resistant to torsion (Figure 3, E) and pressure by elastic deformation of the structure to the applied force (13). On the other hand, the mineralized collagen is responsible for hardness and great compressive strength (Figure 3, B) that collagen fibrils lack (15).

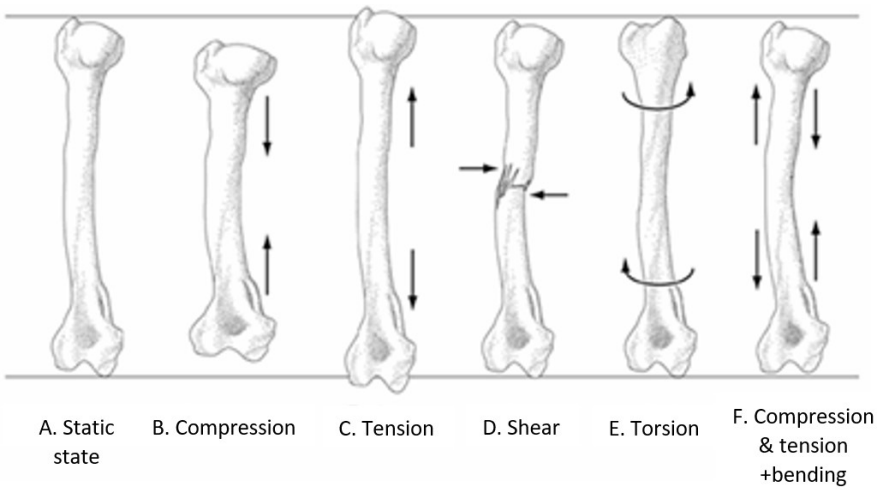

Figure 3: Forces applied to bone. Taken from Troy (16).

The proportion of calcium-deficient hydroxyapatite in dry mineral mass is about 85 %. The second most abundant constituent is calcium carbonate with 10 % of the mineral

mass. The rest mass is formed of magnesium phosphate, calcium fluoride, and calcium chloride. The ratio of organic and inorganic parts is according to the age of an individual. In infants, 48 % of bone mass consist of inorganic salts whereas in elderly the same value reaches 60 %. Calcium-deficient hydroxyapatite, which is present in bone tissue and is securing the mechanical strength, resembles the precipitated hydroxyapatite with the Ca/P ratio between 1,5-1,67. However, the composition of natural bone cement and precipitated hydroxyapatite differs in magnesium and carbonate content that lacks in artificially prepared cement (5).

DCPD, previously mentioned in subsection 3.1: Calcium phosphates, is considered to be the precursor of calcium-deficient hydroxyapatite in human bones and is found in fracture callus in the process of healing (5).

Compressive strength of human bone is an important physical property since it is the main function of bone to withstand compressive forces. In general, the compressive strength is significantly higher than tensile strength and shear strength (Figure 3) where the bone is most susceptible to mechanical failure. The compressive strength varies with sex and age and other factors such as genetics, nutrition, and pharmaceuticals. The mean value of compressive strength for cortical femur bone in males is 141,6 ± 15,91 MPa whereas in females it is 118,91 ± 18,99 MPa (17). The compressive strength of trabecular bone is between 2 and 45 MPa (18).

3.2.2 Healing process of fractures

For the sake of comprehensiveness, the basic physiology of fracture healing must be described. The process of fracture healing in bones is a remarkable example of the vertebrate body capabilities. Healing of bone tissue damage is different from other repairing processes in the human body because healing occurs without forming a fibrous scar.

There are three main repairing mechanisms of long bones in the human body. The specific process which takes place each time depends predominantly on the width of the fracture gap and the presence or absence of movement in the fracture site (19).

Indirect healing is the most common of healing mechanisms. It takes place when a considerable gap is combined with possible movement between fracture ends. In this case, the reparation does not start at the fracture ends. Counterintuitively, an inflammatory reaction causes a hematoma in between and around the fracture ends.

This hematoma forms a template for callus formation. This callus undergoes an endochondral shift from fibrin hematoma to cartilage. For this process, the presence of mesenchymal stem cells is essential (20). These cells are recruited from bone marrow as well as from blood circulation. The growth of cartilage is supported by hypoxia caused by impaired blood flow and by movement in the fracture site (21). After the blood flow is restored by the effect of VEGF and angiopoietins, the cartilage ossification begins by hypertrophy and consecutive cartilage apoptosis. This continues with the export of mitochondrial calcium and its extracellular precipitation as calcium-deficient hydroxyapatite. The mass of chondrocytes is under the effect of several signal molecular pathways e.g., M-CSF, RANKL, OPG, or TNF-α which regulate apoptosis and resorption of callus (22). This newly formed calcified callus is subsequently remodeled by osteoblastic and osteoclastic activity into the lamellar or spongy bone. In lamellar bone, the medullary cavity and Haversian system are formed when the pressure in the axial direction is applied (19).

Contact healing, on the other hand, is achieved when the surfaces of fracture termini fit with a gap less than 0,01 mm and little to no interregional movement occurs. The absence of these factors inhibits the growth of a callus. This type of healing can mostly be achieved under surgical conditions. In this case on the edge of an osteon, a cutting cone of osteoclasts and osteoblasts emerges that restores the Haversian system lengthwise.

If the fracture gap is bigger than 0,01 mm and smaller than 0,8 mm a gap healing process follows. In this case, a lamellar bone is formed like in contact healing. The difference is noticed in orientation. In gap healing, the lamellar bone is created crosswise to the long axis of the bone and must undergo a relatively slow process of remodeling in which the durable long bone restores its function (19).

3.3 Artificial bone cements

3.3.1 PMMA bone cement

Polymethylmethacrylate cement was the first to be used as artificial bone cement and was a significant improvement in bone substitution and artificial joint fixation as well as progress in dentistry (23). PMMA cement paste consists of a solid and liquid phase. The solid phase is usually polymer pellet with the possible addition of X-ray contrast medium and the liquid phase is primarily methyl methacrylate (24).

The connection between cement and bone tissue is the disadvantage of this material and causes complications or even dislocations. PMMA does not occur naturally in the body and there is no mechanism of biodegradation or bioadhesion to human tissue. Moreover, PMMA is toxic when degraded to monomers (9). The obstacle of bioadhesion can be partially overcome by coating the polymer with hydroxyapatite or with silanization (23).

The setting reaction of PMMA is a radical-induced polymerization and is noticeably exothermic. This leads to contact damage of adjacent tissue when exposed to temperatures as high as 100 °C. Additional disadvantages are the thermoplastic behavior of PMMA polymer, the increased plasticity in a water environment, or the reorganization of polymer structure. This reorganization is known as β transition and occurs between room and body temperature. The polymeric structure of PMMA makes it susceptible to creep. This behavior of deflection under constant stress causes changes in anchoring and might eventually cause loosening. The stress relaxation works by the same mechanism as the creep. This process is responsible for reducing tensile stress that is in majority of cases the root cause of the cement failure (25).

The minimal compressive strength for acrylic cement bone implant according to ISO 5833:2002 is 70 MPa calculated from fracture point. The mean value of compressive strength was measured to be 93,0 MPa, though the failure in compressive strength is a scarce cause of complications in PMMA cements (25). PMMA cements are therefore used in more weight-bearing applications such as arthroplasties (26).

As in the case of natural bone, the compressive strength exceeds the tensile and shear strength, but unlike in the bone, the tensile strength is lower than shear strength in PMMA cements.

3.3.2 Calcium phosphate bone cements

Calcium phosphate bone cements are preferable materials for bone repair due to their high bioactivity. They are composed of solid and liquid parts that upon mixing create an injectable paste or are left to harden in a preset form. The solid part usually consists of one or more calcium phosphate derivative powders (e.g., calcium phosphate dihydrate + tetracalcium phosphate or monocalcium phosphate monohydrate + β-tricalcium phosphate or even combination of α-tricalcium phosphate + monocalcium phosphate monohydrate + calcium oxide). The liquid part is without an exception an aqueous solution (water, citric acid solution, or disodium phosphate solution).

Calcium phosphate cements can be categorized into different groups according to their:

- solid-phase composition (tetracalcium phosphates, α-tricalcium phosphate, β-tricalcium phosphate, and others)
- setting reaction (acid-base reaction or hydration)
- the final reaction product (apatite-, brushite-, amorphous calcium phosphate-forming cements) (9)

The major advantage of CPCs over PMMA cements consists in a non-exothermic setting reaction. The exothermic peak of the setting reaction of CPCs is 37 °C (26). Further, final products of CPCs are all biodegradable and could be resorbed by osteoclasts and eventually replaced by bone tissue. This phenomenon is highly dependent on the microstructure and composition of individual CPC (26).

The behavior of different calcium phosphate bone cements depends on their solubility in water. This behavior can be depicted by their isotherms (Figure 4). From this graph, it is noticeable that hydroxyapatite is the least soluble substance under physiological conditions and thus the most stable. The solubility of calcium phosphates except for stoichiometric hydroxyapatite is higher than of natural bone mineral mass, whereas the solubility of hydroxyapatite is lower than of the mineral mass of human bone. Hence, the solubility of precipitated calcium-deficient hydroxyapatite is slightly higher than of synthetic hydroxyapatite (5).

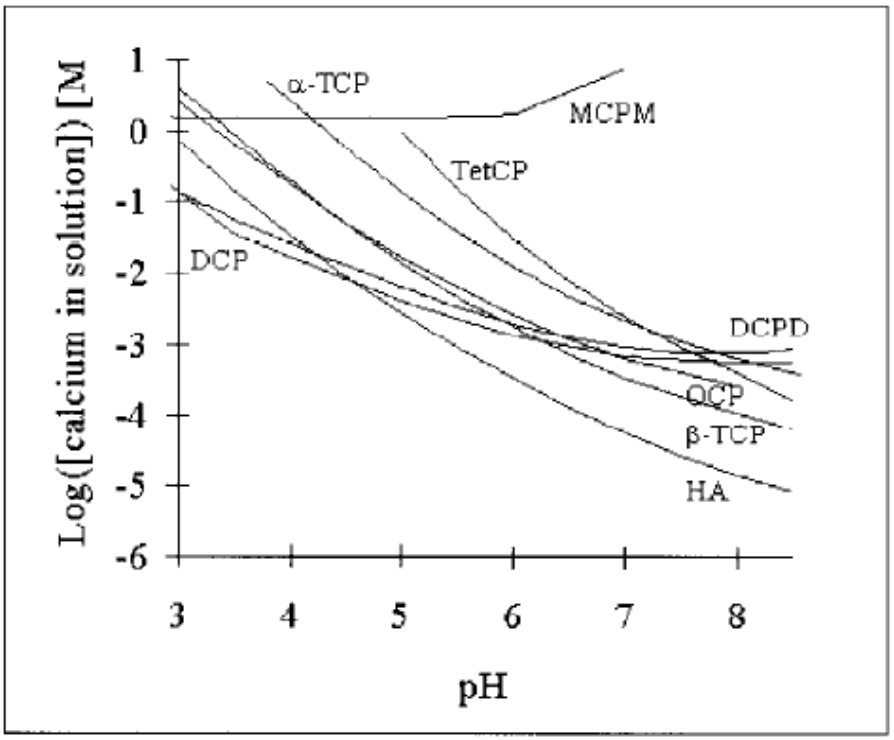

Figure 4: Solubility of Calcium phosphates in water, DCP is dicalcium phosphate, TetCP is tetracalcium phosphate, MCPM is monocalcium phosphate monohydrate, DCPD is dicalcium phosphate dihydrate, OCP is octacalcium phosphate, HA is hydroxyapatite. Taken from Bohner et al. (14).

3.3.2.1 Kinetics of calcium phosphate setting reaction

The solution chemistry of calcium phosphates is most often described by a ternary system; $Ca(OH)_2$ is representing the basic part, H_3PO_4 is representing the acidic part and H_2O is representing aqueous solution. This system is useful for the characterization of CPCs by their solubility and calculations of their solubility product constant. This characterization must be done under laboratory conditions since the addition of any acidic or basic compound shifts the equilibrium. Therefore, this characterization is more an illustration than a definite description of what process is taking place under physiological conditions.

As mentioned in subsection 3.1 Calcium phosphates, the solubility of different calcium phosphates differs. This diversity is depicted by isotherms at 37 °C. In general, the isotherm describes the relationship between the logarithm of the calcium or phosphate concentration versus pH (similar to Figure 4) (4).

The process of precipitation of the most thermodynamically stable product (AX) can be described by the general Equation 2.

$$\frac{\Delta G}{RT} = ln \frac{I_p^{AX}}{K_{sp}^{AX}} = ln\, S \qquad [2]$$

Equation 2: Thermodynamic expression of supersaturation/undersaturation balance of compound AX in solution. Where G is Gibbs free energy, R is the gas constant, T is thermodynamic temperature, I_p^{AX} is the ionic activity of the product, K_{sp}^{AX} is a solubility product constant, S is thermodynamic saturation level. When S<1 the solution is undersaturated relatively to compound AX, when S=1 the solution is saturated and when S>1 the solution is oversaturated. Taken from Fernández et al. (4).

The setting reaction of cement formed by α-tricalcium phosphate is described by Equation 3.

$$3\ \alpha\text{–}Ca_3(PO_4)_2 + H_2O \xrightarrow{\text{pH 7,4}} Ca_9(HPO_4)(PO_4)_5OH \qquad [3]$$

Equation 3: Precipitation of calcium-deficient hydroxyapatite.

In this equation, the α crystalline form of tricalcium phosphate hydrates under physiological pH and forms precipitated calcium-deficient hydroxyapatite. Contrary to other hydration reactions of other simple calcium phosphate compounds, this reaction does not produce free H_3PO_4 or $Ca(OH)_2$ which makes the use of e.g., dicalcium phosphate dihydrate or tetra calcium phosphate unsuitable for clinical application (27).

The process of hydration and formation of cement is a dissolution-precipitation process in which the more soluble calcium phosphate dissolves and, according to pH, the more stable calcium phosphate precipitates. The mechanism of hydration can be divided into two phases as it is shown in Figure 5. The first hydration phase takes place between 5 and 30 minutes after mixing of the solid and liquid phase. The second phase shows a peak for temperatures around 37 °C at cca 12 hours after mixing and is finished after 21 hours (28). Precipitated crystals can later form needles or plates that are responsible for the mechanical function. Each time, due to supersaturation of solution, a crystal of calcium-deficient hydroxyapatite is formed and the equilibrium is reestablished by dissolving more α-TCP (9).

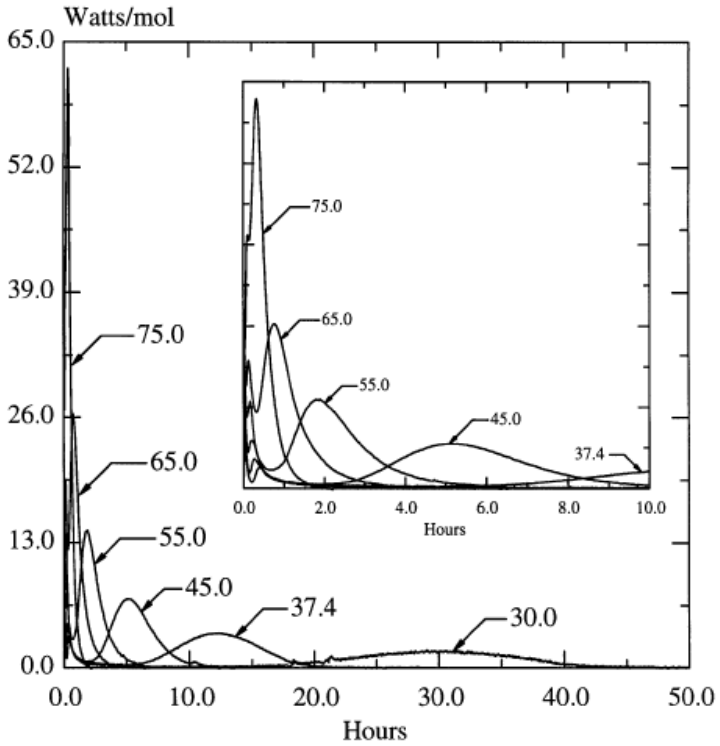

Figure 5: Curves showing the hydration rate of α-TCP at different temperatures. The inserted figure shows the first reaction peak occurring between 5-30 minutes. Taken from TenHuisen et al. (28).

To accomplish the full conversion of α-TCP towards calcium-deficient hydroxyapatite the material must undergo a five-step reaction. These steps are start, induction, acceleration, deceleration, and termination (Figure 6). Each of these steps can be regulated, e.g., the induction phase can be accelerated by the addition of hydroxyapatite nuclei into the solid phase. Further acceleration of calcium-deficient hydroxyapatite formation can be achieved by the use of NaH_2PO_4 or other phosphates or citrate in the liquid phase (9).

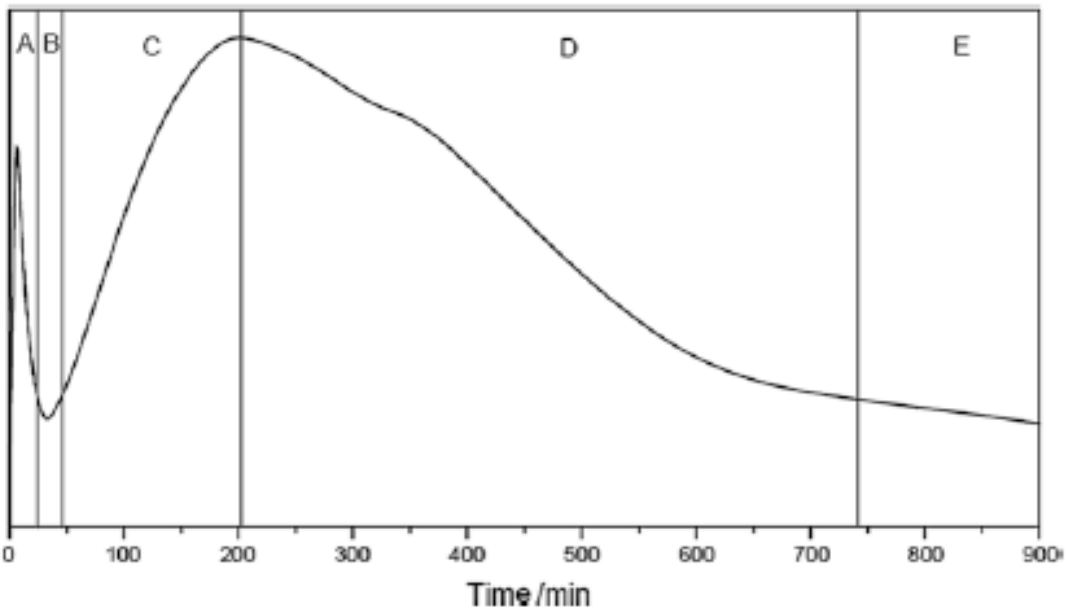

Figure 6: Graph showing steps of cement setting reaction. Rate of energy liberation versus time. A-start, B-induction, C-acceleration, D-deceleration, and E-termination phase. Taken from Chen et al. (9).

3.3.2.2 Properties of calcium phosphate cements

Since the skeletal system is the main load-bearing compartment of the vertebrate body, mechanical strength is the fundamental characteristic that a potential bone substitute must possess. In earlier studies was found that maximum compressive strength of an α-TCP cement could be observed after cca 70 hours setting with values 40,1 ± 1,8 MPa and 34,6 ± 1,0 MPa for different particle sizes (median size 10,88 μm and 2,22 μm respectively) (29). The correlation between compressive strength and porosity is such, that the higher the porosity the lower the compressive strength (30).

Rheological properties of CPCs must mainly allow the paste to be injected and then on-site to mold perfectly in the damaged area. Thus, the low viscosity of the paste is a preferable property. CPC's paste has shear-thinning property and with longer setting time, yield stress increases. Injectability of cements can be also improved by the addition of NaH_2PO_4 (9).

Unlike the PMMA cements and implants, CPCs possess favorable biological properties such as biocompatibility, osteoconductivity, biodegradability, and non-exothermic properties of setting reactions. Due to these facts, cement can be injected, molded, and set *in situ*. This self-setting property offers less invasive surgical procedures and causes a perfect adjustment to the desired area. The biodegradability of CPCs is its major advantage. On the other hand, the rate of resorption must be in equilibrium with the new

bone ingrowth. The resorption of CPCs is executed by osteoclasts, polymorphonuclears and macrophages (18). To achieve this, a certain degree of porosity is required for the cells to invade the side, start the resorption, and to allow neovascularization. The minimal pore size should be 50 μm to achieve neovascularization and 200 μm to allow bone ingrowth. Interconnected pores can be incorporated into cement by the addition of hydrogen peroxide, naphthalene, or polymeric materials (31). Other factors affecting the resorption are Ca/P ratio, crystallinity, crystal magnitude, and wetness (18).

Bioactivity of CPCs is defined as the ability to form strong bonds with human tissue, in this case, bone tissue. Osteoconductivity describes the quality of material that it serves as a scaffold for bone ingrowth. CPCs can promote bone formation in vacant sites even without bone growth factors. This property is called osteoinduction (18).

The safety of the CPCs' final product – hydroxyapatite, in terms of acute toxicity, mutagenicity, and carcinogenic behavior *in vitro* and *in vivo*, was proven by Liu (32). This material did not cause any inflammatory reaction in the damaged site (9).

Despite high bioactivity and osteoconductivity of CPCs, the low resorption rate of calcium-deficient hydroxyapatite is a major disadvantage. Some studies focus on enhancing the resorption by the addition of calcium sulfate or gypsum (10).

3.3.3 Composite calcium phosphate bone cements

Although the CPCs offer interesting properties, the research is now focused on composing materials based on CPCs with additives that would improve its performance in specific parameters e.g., strength, bioresorption, or induction of physiological processes (33). In this part, several possible directions of research are outlined.

3.3.3.1 Silicate substituted CPC

Since the discovery of the silicon role in bones, quite a lot of research has been done on bioglass materials and silicated CPCs. These cements proved to have better biological performance than pure CPCs. This phenomenon is according to some studies occurring due to passive mechanism e.g., change in surface profile rather than by active metabolic influence on osteoblastic or osteoclastic cells (34). The silicon addition is limited and generally does not exceed the boundaries of 0,1 and 5 % of the total mass (35).

The first type of silicate substitution is by the addition of bioglass. Even if this material enhances the biodegradability of formed cement, it is non-biodegradable.

The discrepancy between the properties of cement and bioglass gives rise to additional cracks and pores. The bioglass itself is bioactive and enhances bone growth and regeneration. In addition, it was found to improve mechanical properties (36).

The second silicate substitution type is the silicon addition inside some of the cement phases. Silicon is usually added as silicate form to the solid phase of CPC. This additive can change the properties in a way that new crystals of calcium-deficient hydroxyapatite are lodged in silicate xerogel. Furthermore, silicate doping increases resorbability, cell differentiation, and attaching to the surface along with higher levels of alkaline phosphatase (33). The same cannot be stated about silicate substituted α-TCP; contrary to other CPCs, the addition impairs the reactivity (probably by the formation of an amorphous silica coating) and thus, the biodegradability is even lower than in pure CPCs (37).

3.3.3.2 Magnesium doped CPC

Magnesium ions are by their nature capable of forming a phosphate salt. This fact is exploited in engineering by the use of magnesium cement in construction as a concrete repair material with struvite ($NH_4MgPO_4 \bullet 6H_2O$) being the final product (38). This led to the premise that a combination of magnesium and calcium ions might improve the properties of CPCs. Studies have shown that, except regular hydroxyapatite, magnesium substituted hydroxyapatite and magnesium phosphate can also occur (33).

Compared to pure CPC, the magnesium addition shortens setting time, increases compressive strength, biodegradability, and promotes cell attachment which might be partially caused by increased roughness of the surface (39). Furthermore, it causes the promotion of collagen type I and matrix proteins as well as of proteoglycans. This phenomenon is generally associated with the mineralization of bone tissue (18). Magnesium addition also promotes osteoblast activity (37).

3.3.4 CPC as a drug carrier

Some disorders or traumas that can be treated by injectable calcium phosphate cements are known to be susceptible to pharmacological treatment. Additionally, the fact that a skeletal system is a place where systemically administered drugs with no special affinity to it have difficulties in reaching effective tissue concentrations, makes CPCs an interesting drug carrier candidate studied *in vitro* and *in vivo* (40).

There are four ways of how a drug can be incorporated in the injectable cement:

- it can be dissolved in a liquid phase before mixing of the phases – this offers the evenest distribution of an active substance and faster release (41),
- it can be added to the solid phase before mixing,
- it can be added to the paste of both phases compounded, or
- it can be immersed in a drug solution (this counts for preset cement blocks).

A big advantage of CPCs is that the setting reaction is non-exothermic and thus even thermolabile drugs e.g., biopharmaceuticals, can be loaded. On the other hand, the setting environment is known for its pH changing. This must be taken into consideration when choosing a pH-sensitive molecule (42).

The properties of each drug-loaded CPC rely strongly on the internal structure of the cement (i.e. surface area, porosity, permeability), its disintegration, and interaction between the active substance and cement. The mechanical strength and rheology of a drug-loaded cement must be experimentally determined for each formulation and cannot be predicted (42). Usually, the addition of a drug tends to prolong setting time and might even inhibit crystal growth. This is due to the chelation of calcium ions or by adsorption of carboxylic groups to the hydrating phase (43).

CPCs act as non-swelling and non-eroding systems; hence the drug liberation relies solely on diffusion from the system while the system stays rigid. For this characteristic of a matrix, a Higuchi's model and potentially also Korsmeyer-Peppas and Weibull's are applicable. Active substances tend to show a burst effect within hours after immersion during their dissolution (44). This can be avoided either by the addition of polymers or silicon (43).

So far, a plethora of different active substances was examined by various authors. Among others, antibiotics (e.g., amikacin, flomoxef, gentamycin, tetracycline), NSAIDs (e.g., acetylsalicylic acid, indomethacin, ibuprofen), cytostatics (e.g., cisplatin, methotrexate, doxorubicin), bisphosphonates (e.g., alendronate, pamidronate), growth factors (e.g., BMP, TGF-β, FGF), ions (e.g., calcium, phosphate, magnesium, strontium) were added in different CPCs (42).

3.4 Characterization techniques

In the experimental part of this work, the following characterization techniques were used.

3.4.1 Injectability

Bohner et al. define the injectability of a paste as ‘‘*Capacity of a material to stay homogenous during injection, independent of the injection force*’’ (45). However, authors predeceasing Bohner used other definitions e.g., “*with constant force applied*” (46). In this work, the Bohner’s definition was used since the main aim was to prepare a paste that could be injected by finger pushing the syringe plunger during a surgery. During the injectability test, the paste is inserted into a test syringe and, by applying a force to the plunger, the paste is expelled through the syringe tip. The paste must stay homogenous i.e. without phase separation. As earlier stated, for the purposes of this work injectability was studied as a qualitative capacity followed Bohner's definition. However, injectability is by some authors quantified as in Equation 4.

$$Injecability\ (I\%) = \frac{Mass\ expelled\ through\ syringe\ tip}{Total\ mass\ before\ injecting} \qquad [4]$$

Equation 4: Injectability, taken from O'Harra et al. (47).

Figure 7: Injectability test. Taken from Brunner et al. (81).

3.4.2 Washout resistance

Resistance to washout is a quality of a paste to maintain cohesion after immersion in an aqueous/physiological environment without releasing cement particles. The solution is, in the qualitative method, observed by naked eye and disintegration and turbidity is evaluated. The quantitative assay consists of mass loss measurement after immersion into a liquid (9).

3.4.3 Raman spectroscopy

‘‘*Raman spectroscopy is a spectroscopic technique used to detect vibrational, rotational, and other states in a molecular system, capable of probing the chemical composition of materials*.’’ (48).

Raman spectroscopy relies on inelastic scattering of a monochromatic laser beam that interacts with the examined material. This interaction consists of absorption of the energy of the laser beam by the sample, change of the form of energy into rotational or vibrational energy of sample molecules, and subsequent release of a light photon with shifted frequency. This photon is detected by a photodiode and Raman shift is evaluated (49).

Molecules depending on their absence or presence of Raman active modes emit different wavelengths photons. In the case of the absence of Raman active modes, the emitted photon bears the same frequency as the absorbed photon. This phenomenon is called Rayleigh scattering and is observed in 99,999 % of interactions. On the other hand, if the molecule is Raman active it can either absorb energy and emit a photon with lower ‘‘Stokes’’ frequency, or the molecule can be already in higher energy state and the emitted photon bears higher ‘‘Anti-Stokes’’ frequency (50). For graphic explanation see Figure 8.

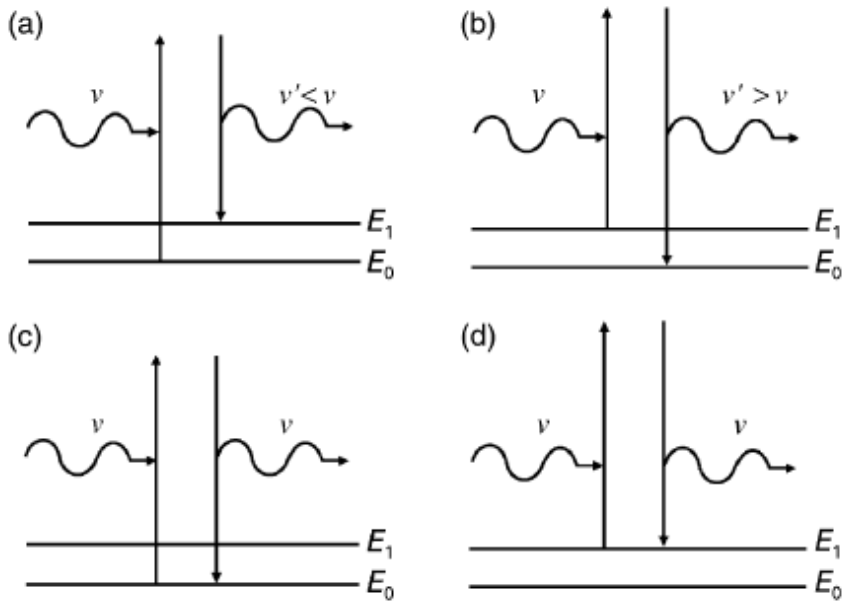

Figure 8: Depiction of energy levels during Rayleigh and Raman scattering. Impinging photon is on the left, emerging photon on the right. (a) depicts Stokes transition, (b) Anti-Stokes transition, (c) and (d) Rayleigh scattering. Taken from Andrews et al. (82).

The outcome of Raman spectroscopy is a graph where on the y-axis is the intensity of signal against wavenumber (reciprocal wavelength) on the x-axis. Spectra obtained by Raman spectroscopy give information on the frequencies of vibrations occurring inside the molecules of the sample. Molecular groups are depicted by their characteristic bands often referred to as a spectral fingerprint. The method is complementary to FT-IR since the Raman active molecular bonds often absorb faintly in the IR e.g., aliphatic chains, disulfide bond, aromatic ring, or C=C bond (50).

Raman spectra of α-TCP and calcium-deficient hydroxyapatite can be used for qualitative monitoring of the hydration and precipitation reaction occurring during the hardening of CPC (51).

3.4.4 X-ray diffraction

X-ray diffraction is an analytical method using monochromatic X-ray photons for non-destructive analysis of the crystal lattice, molecular positions, spacing angles, crystal size, residual stress, dislocation density, and for material identification. This important technique relies on the interference of X-rays upon impingement on a sample, where, in case anisometric crystal behavior is present, constructive interference occurs. On the other hand, if isotropic amorphous behavior is present, there is no detectable constructive interference although diffraction is still present. Short crystal patterns show

diffraction at small angles whereas long periodical intervals show diffraction at higher angles (52).

A diffractogram is presenting intensity plotted against the angle between the incident X-ray and the diffracted X-ray in 2θ (Figure 9). The position on the x-axis describes the qualities of the unit cell i.e. size and shape whilst the intensity of the signal denotes proton number and atom position inside the unit cell. The fundamental equation for XRD is the Bragg's equation (Equation 5).

$$n\lambda = 2dsin\theta \quad [5]$$

Equation 5: Bragg's equation where, n= integer in order of reflection, λ= photon wavelength, d= lattice distance, θ= angle of impinging photon. Taken from Ameh et al. (52).

Powder X-ray diffraction method is used for the characterization of polycrystalline mixtures. Since every material diffracts the beam in its unique fingerprint pattern a database by Joint Committee on Powder Diffraction Standards (now ICDD) is stored for comparison of sample material patterns. The X-ray source is typically a cathode-ray tube emitting polychromatic X-rays. Since the Bragg's equation is applicable for one wavelength exclusively a monochromator is used. Beam impinging on the sample is scattered, refracted, diffracted, transmitted, and absorbed. Diffracted beams from different crystal planes are parallel and detected at a 2θ angle relative to a transmitted beam (53). A schematic representation of the X-ray diffractometer is shown in Figure 9.

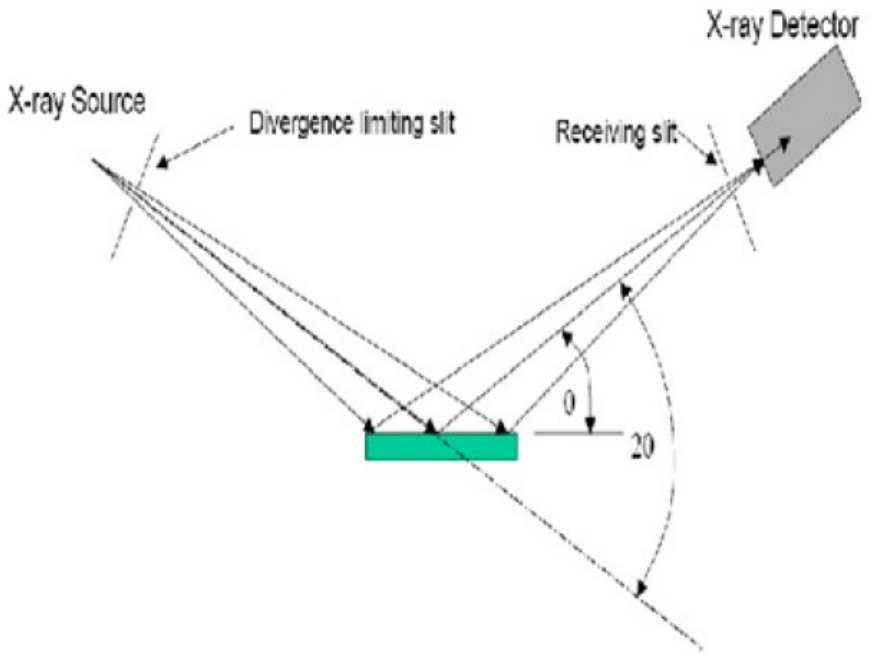

Figure 9: Scheme of XRD. The green rectangle represents the sample. Taken from Sharma et al. (54).

3.4.5 Compressive strength

Compressive strength (σ) testing is a technique of materials science used to determine the material's resistance to uniaxial crushing. The testing machine creates pressure which ultimately leads to the break of the examined material. After a finite section of elastic deformation where Hook's law is applicable, the load-displacement curve culminates at the yield point. From thenceforth the deformation is plastic and the material does not restore its original dimensions (55). The fundamental equation for compressive strength is Equation 6.

$$\sigma = \frac{F}{A} \qquad [6]$$

Equation 6: Equation of compressive strength, where σ represents compressive strength, F represents force and A represents the area.

The testing can be carried out by measuring the complete load-displacement curve or by recording only the highest value i.e. failure load or yield point. The pressure can be applied at a constant value or at a constant increment of increasing load or at a constant displacement rate (55).

3.4.6 Dissolution testing

Dissolution is a measurable process during which a drug or other solute is dissolved into a solvating medium. A drug is transferred from its solid form into an unsaturated liquid medium surrounding it. The fundamental controlling mechanisms of dissolution are the surface area of a solute, dimensions of the boundary layer, diffusion coefficient, and solvent medium. The dissolution rate also depends on solute particle size, mixing of the solvent, solvent's viscosity, and temperature (56). Equation 7 is describing the dissolution rate.

$$\frac{dC}{dt} = D \times A(C_s - C) \qquad [7]$$

Equation 7: The dissolution rate described as a change in the concentration over time. dC represents the change in concentration, dt represents the change in time, D represents diffusivity coefficient, A represents the surface area, Cs represents solute solubility and C concentration. Taken from Bruschi et al. (56).

In vitro dissolution testing of a non-solution drug-loaded dosage form is a mandatory requirement of every medicine registered in the EU. Ph. Eur. harmonized the dissolution testing with USP and JP. Four types of testing apparatuses are specified in the Ph. Eur. and are approved as methods for registration of drugs. Those are Apparatus 1 – Basket apparatus, Apparatus 2 – Paddle apparatus, Apparatus 3 – Reciprocating cylinder

apparatus, and Apparatus 4 – Flow-through cell apparatus. Modifications specified in the pharmacopoeia can be realized to suit specific dosage forms (57). Although these apparatuses are required for FDA or EMA registrations, research is not obliged to use them.

Since the rate of dissolution of calcium-deficient hydroxyapatite is insignificant compared to the dissolution of model drug – ibuprofen, a Higuchi's model can be used to describe at least partially the dissolution from calcium phosphate cement matrix (57). Higuchi's equation is shown in Equation. 8.

$$\frac{W_r}{t_{1/2}} = 2W_0 \frac{S}{V}\sqrt{D/\pi\tau} \qquad [8]$$

Equation 8: Higuchi's equation: W_r = amount of drug dissolved over time t, W_0 = dose of the drug, S = effective diffusional area, V = volume of a hydrated matrix, D = diffusion coefficient of the drug, τ = tortuosity of the matrix. Taken from Uddin et al. (57).

During the process of dissolution, samples of the dissolution media are taken and analyzed by a suitable analytical method. This can be done either online with analysis succeeding the collection of the sample without delay or offline with analysis independent on the sample collection (58).

3.4.7 UV/VIS-spectrophotometry

Spectrophotometry of the ultraviolet and visible part of electromagnetic spectra is a qualitative and quantitative analytical method. It can be used for the identification of specimens as well as for quantitative measurement of drug concentration by measuring absorbance or transmittance of the sample at a specified wavelength often succeeding dissolution testing and/or HPLC extraction (59).

The technique depends on the absorption of electromagnetic radiation mainly by π electrons of the sample molecules. Since a considerable number of drugs contain double, triple bonds or even resonance arrangement in their structures which absorb mainly ultraviolet and visible rays, UV/VIS spectrophotometry is often a method of choice. Lambert-Beer's law describes absorbance as the product of the molar absorption coefficient, concentration, and optical path length (60). The absorbance equation is shown in Equation 9.

$$A = \varepsilon \times c \times b \qquad [9]$$

Equation 9: Lambert-Beer law. Where A represents absorbance, ε represents molar absorption coefficient and b represents optical path length. Taken from Klimeš et al. (60).

For qualitative identification, it is necessary to perform the analysis under pharmacopoeia defined conditions. For quantitative analysis, a calibration curve of standard solutions is required. This involves preparing a set of defined concentrations solutions, measuring them against a blank sample, and subsequent generating an equation describing the calibration curve at a sufficient coefficient of determination. In quantitative analysis usually, absorbance (on the y-axis) is plotted against drug concentration (on the x-axis) (59).

3.4.8 Scanning electron microscopy

Scanning electron microscopy is an advanced imaging technique relying on the interaction of an electron beam on a sample surface. Images depict surface topography, morphology, and if energy dispersive X-ray detector is mounted, also microchemical analysis with peaks of intensities of elements. It enables seeing details with useful magnification up to 200000x compared to common light microscopy with useful magnification around 1000x. This is mainly due to the fact that the limiting factor of light microscopy is a large wavelength of light (400-800 nm), whereas in electron microscopy the wavelength of the electron beam can be, depending on the accelerating voltage, around 4 pm. For objects smaller than 200 μm light microscopy is no longer useful and either scanning or transmission electron microscopy must be used. Limitation of scanning electron microscopy lies in that a sample must be conductive, thus sputter coating with gold, platinum, chromium, tungsten, tantalum, or carbon must precede the imaging of non-conductive materials such as ceramics. On the other hand, the non-transparency of the specimen does not limit the specimen width as in light or transmission electron microscopy (61).

The main principle of SEM is that a beam of electrons is produced by an electron gun and then propagates through the vacuum of an electron column. Passing through a set of copper-iron electromagnetic lenses, apertures, and coils further focus the electron beam up to 5000 times. Reaching a specimen chamber, the electron beam hits a sample placed on a sample holder attached to a sample stage. The beam collides with the sample surface and then reflects and backscatters electrons and emits X-rays. This radiation is subsequently detected either in the sample chamber or above the lens and is analyzed to form an image of the specimen (61). For a scheme of an electron microscope, see Figure 10.

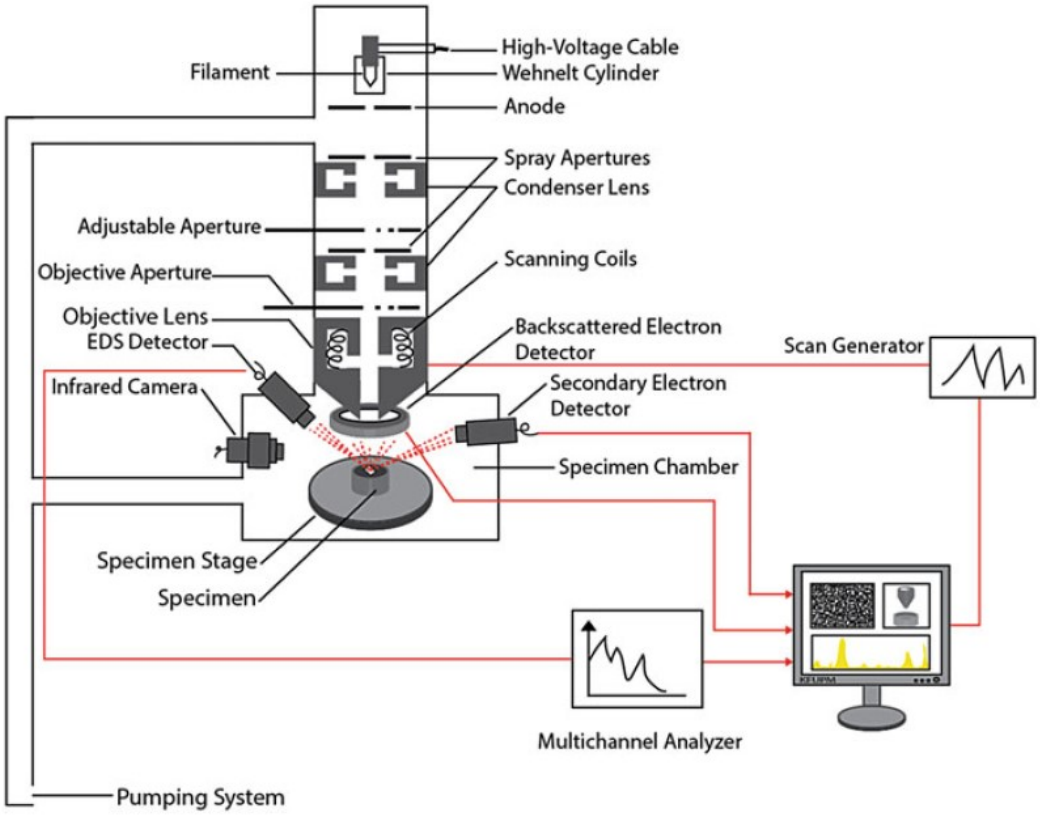

Figure 10: Scheme of a Scanning electron microscope. Taken from Ul-Hamid et al. (61).

4. Experimental part

4.1 Equipment

All the equipment that was used in this work was allocated at the Department of Material Sciences at the University of Patra, Greece and FORTH institute in Patra, Greece.

4.1.1 Devices

Analytical balance Kern, max 120g, d=0,1

Ball mill Fritsch Pulverisette 6

Furnace Nabertherm

X-ray diffractometer Bruker D8

Laboratory incubator shaker with water bath BIOline Scientific

Ultrasound bath Bransor 2510

Sputter coater Emitech K500X

Scanning electron microscope EVO MA 10 Zeiss

Spectrometer Perkin Elmer Lambda 35 UV/VIS

4.1.2 Chemicals

Calcium carbonate ($CaCO_3$), M=100,09, Alfa Aesar

Calcium pyrophosphate ($Ca_2P_2O_7$), M=254,1, Alfa Aesar

Natrium chloride (NaCl), M=58,44, Penta

Kalium chloride (KCl), M=74,55, MERCK

Kalium dihydrogenphosphate (KH_2PO_4), M=136,09, MERCK

Sodium hydrogenphosphate (Na_2HPO_4), M=141,96, Alfa Aesar

Ibuprofen ($C_{13}H_{18}O_2$), M=206,28, MERCK

Ringer solution, B.Braun

Normal saline solution, B.Braun

4.2 Synthesis and characterization of pure α-TCP cement

4.2.1 Synthesis of α-TCP

Since pure α-TCP is the fundamental reactant in the whole cement forming process, it was synthesized with high precision. 25,0062 g of calcium carbonate and 63,4000 g of calcium pyrophosphate were weighed on the analytical balance. The raw material in the form of crystals was mixed and ball-milled in Ball mill Fritsch Pulverisette 6 at 150, 200, 300, 400, and 500 RPM. Each mixing performed in three cycles and each cycle was for 10 minutes. The material produced during the process, due to high friction forces, had to be scraped out of the agate walls of the grinding bowl after each execution. The intensive process of milling also secured a precise mixing of the two aforementioned chemicals.

The mixture was transferred into an aluminum oxide crucible capable of withstanding temperatures up to 1450 °C which are taking place in the furnace during the reaction process. The material was mixed with acetone and shaped to reduce the contact surface. The crucible containing the mixture was put into a furnace and warmed up to 1450 °C for 8 hours. The temperature was held stable for 48 hours. This temperature secured the formation of α-TCP with a negligible contribution of β-TCP.

The synthesis reaction is described by Equation 1.

$$CaCO_{3\,(s)} + Ca_2P_2O_{7(s)} \xrightarrow{1450\ ^oC} Ca_3(PO_4)_{2(s)} + CO_2(g) \qquad [1]$$

Equation 1: Synthesis of α-TCP.

When the reaction was finished, the crucible was quenched in the air on a metal plate. The quenching process ensured the high purity of α-TCP by reducing the time when the mixture was at the temperature suitable for the formation of the thermodynamically more stable β-TCP. After quenching, the raw α-TCP, which is in a compact ceramic state, was crushed by a hammer and put in the Pulverisette ball mill. The milling was performed at 200 RPM for 20 minutes (1 cycle), 300 RPM for 20 minutes (1 cycle), and at 550 RPM for 10 minutes (3 cycles). The material was being scraped out of the walls after each repetition. The finely milled powder of α-TCP was sieved into a plastic container to firstly notice any unground material and secondly to abrade the material stuck to the agate balls. The total mass of α-TCP powder was 71,20 g.

4.2.2 Setting reaction of pure cement

The cement formation is dependent on the solid and liquid phase of cement paste. In this work pure α-TCP powder was used as the solid phase and 4% w/v Na_2HPO_4 aqueous solution as the liquid phase. The Na_2HPO_4 solution was prepared in the laboratory and stored at 8 °C.

The solid phase was transferred to a plastic boat and a sufficient amount of liquid phase was added. Generally, it was 1 g of solid-phase per 0,32 ml of the liquid phase. Nevertheless, this amount varied from experiment to experiment. The ratio between the solid and liquid phase was not the cornerstone of the experiment but the paste consistency was. The ratio of phases was also case-dependent because the paste tended to dry over time and become crumbly which could be reversed only by adding more liquid phase. The different phases were always mixed by a metal spatula.

The well-prepared cement paste was then put in molds of 6 x 12 mm dimensions and 3 balls with 5 mm diameter were formed.

4.2.3 Hardening of pure cement

The process of hardening i.e. process of intertangling of newly formed hydroxyapatite needles and planes took place in a liquid aqueous environment. In this work phosphate buffer solution, Ringer's solution and normal saline solution were used as the media which simulated the extracellular environment of the human body. 1 liter of phosphate buffer solution was prepared from 8 grams of NaCl, 0,201 grams of KCl, 0,245 grams of KH_2PO_4, and 1,42 grams of Na_2HPO_4 and 990,134 grams of distilled water and the pH of the solution was subsequently adjusted to 7,4 by few drops of HCl.

During the washout resistance experiment, the hardening took place in the medium immediately after the cement paste was formed since the nature of this experiment demanded this procedure. In other experiments i.e. compressive strength and blank control for dissolution experiment, the cement paste was initially let to set the shape in molds with dimensions 6 x 12 millimeters for 24 hours at 37 °C at 100% humidity environment. From thenceforth, the samples outside of the molds were stored in PBS at 37 °C. For experiments of compressive strength, Raman spectroscopy, X-ray diffraction, and SEM the intervals of hardening were 1 day, 9 days, 15 days, and 17 days.

The process of hardening i.e. formation of new crystals of precipitated calcium-deficient hydroxyapatite is described by Equation 3.

$$3\ \alpha\text{–}Ca_3(PO_4)_2 + H_2O \xrightarrow{pH\ 7,4} Ca_9(HPO_4)(PO_4)_5OH \qquad [3]$$

Equation 3: Precipitation of calcium-deficient hydroxyapatite.

4.2.4 Characterization of pure cement

The material throughout the process of hardening was examined by several characterization techniques, elucidating the ongoing changes in the microstructure of cement.

4.2.4.1 Injectability

Injectability of the cement (as the least standardized feature) was carried out by inserting the cement paste to a needleless syringe and squeezing it out by applying pressure not exceeding the one potentially performed during a possible medical application. The cement paste was observed on a hard and contrast surface to notice any sign of phase separation or other material changes that would make the paste incompatible for medical use.

4.2.4.2 Washout resistance

The ability of the material to retain its shape without disintegration or releasing its debris was inspected by immersing three ball-shaped samples with a diameter of 5 millimeters in PBS, Ringer's, and normal saline solutions. The ability to retain its shape was evaluated by observing released particles, color changes, transparency, and turbidity of media or changes in the shape of the original samples.

In this work qualitative method presented by Takagi et al. was used (62).

4.2.4.3 X-ray diffraction

Method of X-ray diffraction was executed at the FORTH institute in Patra, Greece. The instrument used was Bruker D8 X-ray diffractometer, as additional equipment agate mortar and pestle were used for grinding the samples.

Crushed samples from compressive strength experiments were further ground to relatively fine brash that was suitable for diffraction experiments.

Diffractograms obtained during the experiments were adjusted by software to correct the baseline and to find matching standards for obtained diffraction spectra with a color highlight of peaks defining the crystal structure. The 2θ angle at which the diffractometer was measuring was set between the range 3° and 70°. From previous experience, no significant peaks had ever been noticed in the past at angles lower than 10° and higher than 60°.

The scanning speed was set to 0,35 seconds/step. The lamp was characterized by Cu Kα radiation, 40 kV voltage, 40 mA current, and wavelength of λ=0,1540598 nm. The source of radiation and detector were both moving to -θ and θ respectively in Bragg-Brentano geometry.

4.2.4.4 Raman spectroscopy

Raman spectroscopy experiments were also conducted in collaboration with the FORTH institute in Patra, Greece.

X-ray diffraction and Raman spectroscopy are both non-destructive techniques., Thus, the samples measured by Raman spectroscope were the same used for the X-ray diffraction experiment. The Raman spectroscope had to be first calibrated to a silicone standard of 520 cm^{-1}. Since the setting shift of the spectroscope was 504,61 cm^{-1} the total adjustment of spectra was 15,39 cm^{-1}.

The pure α-TCP powder that did not undergo any hardening was recognized as a standard of α-TCP while a standard of calcium-deficient hydroxyapatite was available in the laboratory. Raman spectra of standard calcium-deficient hydroxyapatite, α-TCP, and a sample of pure cement after 9 days of hardening were measured under the same conditions.

The juxtaposition of these spectra provided information about the transformation occurring in the samples from α-TCP to calcium-deficient hydroxyapatite.

4.2.4.5 Compressive strength

Compressive strength was measured at a Compressive strength tester. The measured samples were previously let to harden in PBS and, at specific intervals, they were taken to be measured. Dimensions of samples were first measured by a caliper with accuracy to hundredths of a millimeter, for the subsequent calculations of pressure to be precise.

The tester was capable of measuring the whole strain-stress curve, but in this work, only failure load converted to pressure (compressive strength) was used.

Cylinders (gently cleaned by a brush) were placed in the clamp of compressive strength tester and peak deformation forces were recorded for each interval of hardening 3 or 4 times depending on the coherence of results. The crushed material was later used in other experiments i.e. Raman spectroscopy, X-ray diffraction, and SEM.

4.2.4.6 Scanning electron microscopy

For microstructure morphology observation, concretely growth of needles and plates of hydroxyapatite, the scanning electron microscopy was chosen. The SEM instrument which was present at the department of material science was a medium resolution EVO MA 10 Zeiss based on thermal emission tungsten unit (maximum resolution: cca 50000x).

The crushed samples from compressive strength experiments were glued by silver paste to carbon targets and followingly sputtered by gold on Sputter coater Emitech K500X. Different fragments of cements were oriented to show the inner or outer surface of cement during the whole process of hardening.

4.3 Synthesis and characterization of ibuprofen enriched cement

For experiments with ibuprofen enriched cements, α-TCP from pure cement synthesis was used with the addition of 4 % of ibuprofen. The mixture of these was used as the solid phase, the liquid phase was an aqueous solution of 4% w/v Na_2HPO_4.

4.3.1 Setting of enriched cement

The setting reaction of ibuprofen enriched cement was fairly similar to the one without ibuprofen. One of the differences was that the ibuprofen made the solid phase more hygroscopic and the ratio of 1 g of solid phase to 0,32 ml of 4% solution of Na_2HPO_4 had to be adjusted to a larger volume of liquid phase for the cement paste to have proper texture. The cement paste was prepared in a plastic boat and phases were mixed by a metal spatula. The paste had to be quickly transferred into molds to prevent evaporation of liquid and thus changing the solid to liquid phase ratio. Two types of molds were used, first was cylindric of dimensions 6 x 12 mm and second was a tablet blister. Blister molds were chosen to fit 1 gram of cement paste, thus every tablet contained 40 mg of ibuprofen. These tablets were used for the dissolution profile of ibuprofen from cement.

4.3.2 Hardening of enriched cement

The measurement conditions were the same as the conditions for pure cement.

4.3.3 Characterization of enriched cement

4.3.3.1 X-ray diffraction

The measurement conditions were the same as the conditions for pure cement.

4.3.3.2 Compressive strength

The measurement conditions were the same as the conditions for pure cement.

4.3.3.3 Scanning electron microscopy

The measurement conditions were the same as the conditions for pure cement.

4.3.3.4 Dissolution of ibuprofen

To show the dissolution characteristics of cement tablets, five tablets from which four contained 40 mg of ibuprofen and one contained 0 mg as a blank sample, were made in a tablet blister. Each tablet was placed after 24 hours of setting its shape in a 100% humidity environment to an individual vial with 15 ml of PBS. Vials were stored in a Laboratory incubator shaker with a water bath at 37 °C. After time intervals of 3, 6, 9, 24, 48, 72, 120, 168, 264, 432, and 504 hours the PBS solution containing dissolved ibuprofen was transferred into an individual plastic 50 ml centrifuge tubes. Tubes were stored at 7 °C in a fridge until they were measured on a spectrophotometer.

4.3.3.5 UV-spectrometry

The absorption spectrum in the UV field was measured for ibuprofen with two maxima found and used for subsequent measurements. The maxima were at 264,3 nm and 272,8 nm. A calibration curve for concentrations from 5 µg/ml to 400 µg/ml was prepared with 10 points of calibration and R^2=0,9994 and 0,9993 respectively for each wavelength. For the measurement, the slit width was set to 2 nm, the scan speed was 960 nm/min and pure PBS solution was used as a blank sample. The previously obtained solutions, at specific time intervals from the dissolution test, were measured at both wavelengths. The dissolution profile of tablets containing 40 mg of ibuprofen was determined.

5. Results and discussion

5.1 Synthesis of α-TCP

In the first step of this work, the synthesis of reagent took place as described in the experimental part. The yield of the reaction was 91,96 %. The quality of α-TCP ceramic and later powder was examined by X-ray diffraction. For comparison reasons, standard spectra of α-TCP and main byproduct β-TCP were plotted laterally. The contamination by β-TCP is visible on one peak present in the sample line. The absence of major peaks characteristic for β-TCP determines the high quality of the α-TCP powder. For details see Figure 11.

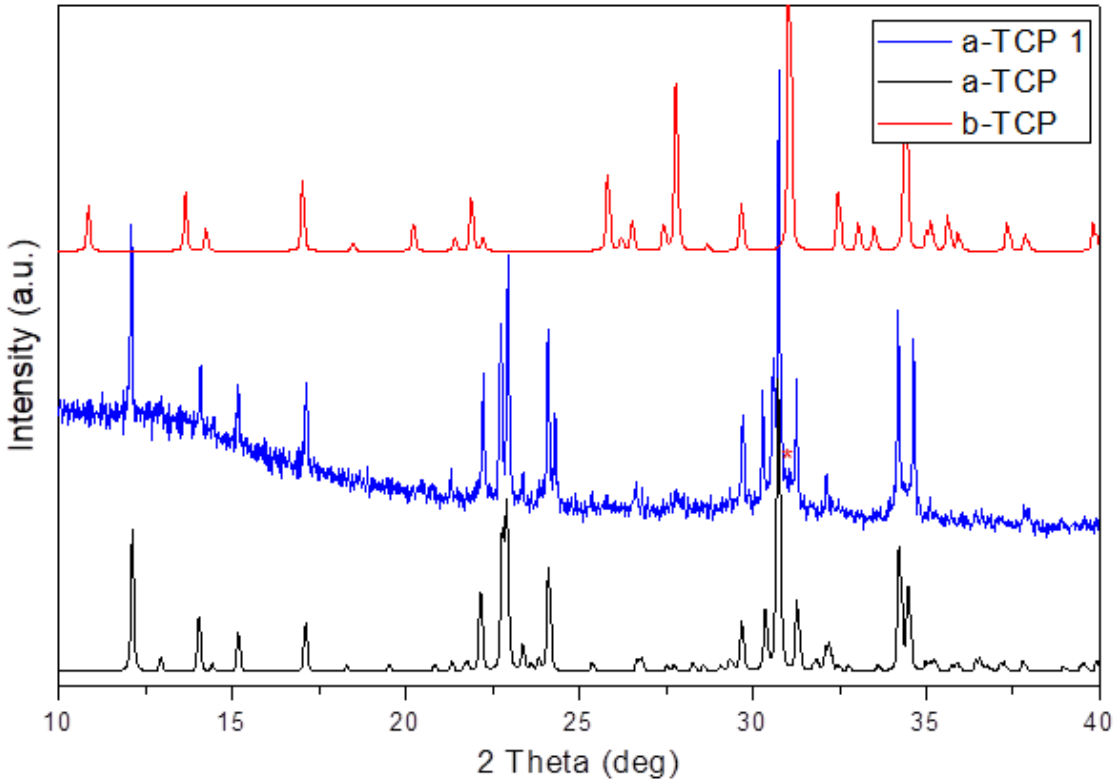

Figure 11: Diffractogram of the sample (blue), standard α-TCP (black), and standard β-TCP (red). A small peak showing β-TCP contamination is marked with a red asterisk.

A high-quality precursor material is crucial for obtaining a cement of desired quality. From the obtained diffractograms can be concluded the α-TCP was of very high quality. The negligible peak at 31,5° θ shows very low content of β-TCP impurity. Very few studies present the diffractograms of their precursor powders. On the other hand, useful information can be extracted from the diffractogram of the cement at t=0 hours. In a previous study, an α-TCP cement with declared purity over 85 % was presented (29). By comparing the height of the β-TCP peak with the same peak from the current thesis

at time t=0 hours, it was easy to conclude that the precursor of this thesis had a lower β-TCP impurity. Thus, purity higher than 85 % was suggested. In another study, an α-TCP cement that at t=0 hours possesses a very similar pattern as the α-TCP synthesized in this work is presented (63). In that case, the impurity content was 11 % of β-TCP which can be the case for this work also. For a more accurate calculation of β-TCP content, additional experiments need to take place with the exact quantification by an external standard.

5.2 Hardening of cements and X-ray diffraction

Changes in the crystalline structure, the hydration reaction of α-TCP, and the growth ofcalcium-deficient hydroxyapatite crystals were examined by XRD. Diffractograms obtained during hardening i.e. 1, 9, 15, and 17 days for both pure (Figure 12) and ibuprofen-loaded (Figure 13) cements. The diffractogram of pure α-TCP is shown earlier (Figure 11). The characteristic α-TCP peak at 23° in Figure 11 gradually diminishes throughout the hardening in Figures 12 and 13. Another peak at 24°, which is also characteristic for α-TCP, diminishes very quickly and is visible only in the first measurement. The peak at 26° is, on the other hand, distinctive for calcium-deficient hydroxyapatite and during the hardening becomes more noticeable. Transformation of α-TCP to calcium-deficient hydroxyapatite is also apparent at 31° and 34° where characteristic peaks for α-TCP weaken throughout the hardening. All these phenomena are due to the formation of calcium-deficient hydroxyapatite and the consumption of α-TCP and are common for both pure and ibuprofen-loaded cements.

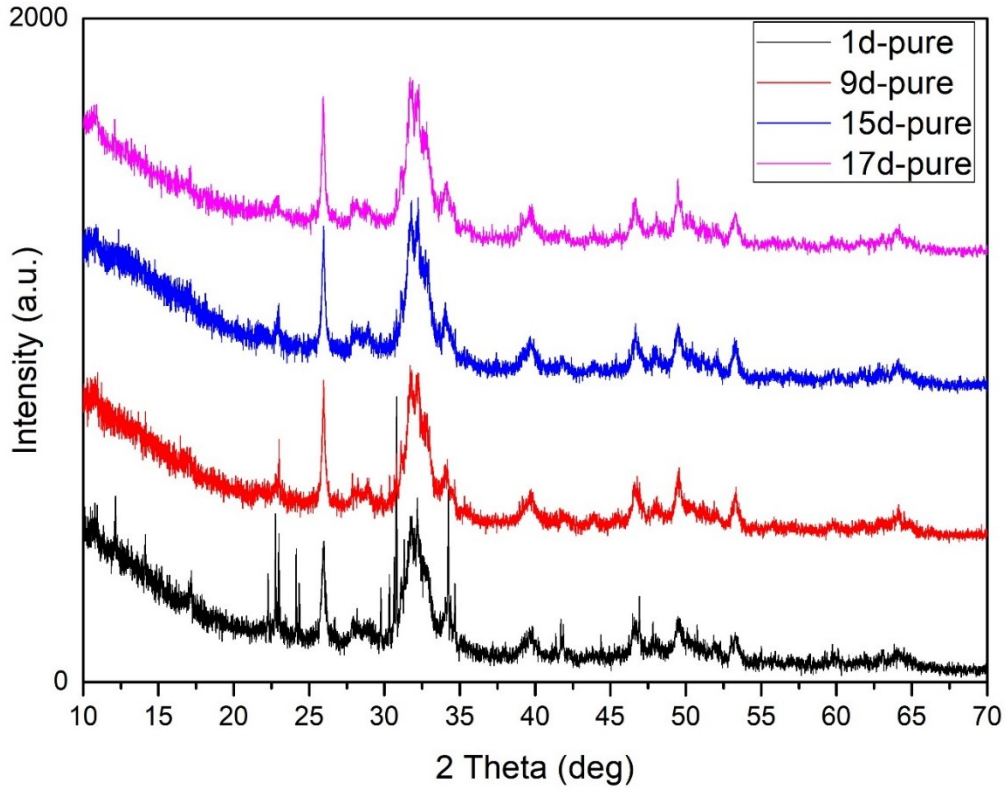

Figure 12: Diffractograms depicting the change in the crystalline structure throughout the hardening of pure cement. The intensity of the signal plotted against 2θ angle.

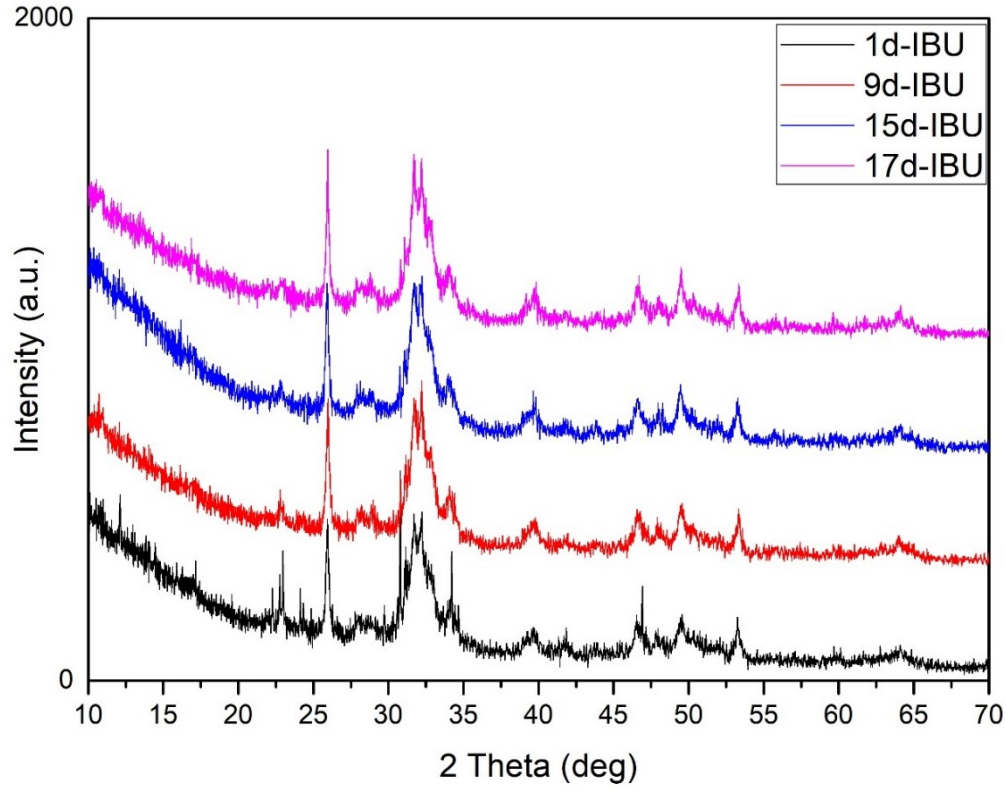

Figure 13: Diffractograms depicting the change in the crystalline structure throughout the hardening of ibuprofen-loaded cement. The intensity of the signal plotted against 2θ angle.

The transition of α-TCP to calcium deficient hydroxyapatite appears to be of the same speed in pure cement as in ibuprofen-loaded cement considering the height of peaks specific to α-TCP and calcium-deficient hydroxyapatite. The conversion is completed after 17 days as it can be concluded from the disappearance of peak at 23° (it is still apparent after 15 days of hardening). The peak at 31° which is considered by Cardoso et al. as the cornerstone of α-TCP presence (63), is hardly visible even after 15 days of hardening. The greatest decline was observed between day 1 and day 9. An important note is also that the diffractogram after only one day of hardening implies a high concentration of calcium-deficient hydroxyapatite e.g., a high peak at 32°. Ginebra et al. showed that the full conversion for a similarly fine powder of α-TCP was achieved after 36 hours of hardening (29). After 64 hours no signs of α-TCP presence were observable. This fast hardening was probably accelerated by the addition of 2 % of hydroxyapatite seeds, which cause faster crystallization of calcium-deficient hydroxyapatite. Takagi et al. claimed that a cement composed predominantly from α-TCP showed almost full conversion after 1 day of hardening (62). The accelerated hardening was probably due to a higher concentration of Na_2HPO_4 which is known to increase the speed of crystallization. Takahashi et al. referred full conversion after 120 hours of hardening (64). In the latest case, cement was based on α-TCP with the addition of Y_2O_3 doped zirconia, Al_2O_3, and SiO_2.

5.3 Injectability

Injectability was successfully tested under laboratory conditions. The paste ran through the syringe hub smoothly without any detectable phase separation. Thus, the injectability of the cement paste was characterized as sufficient without actual value measured.

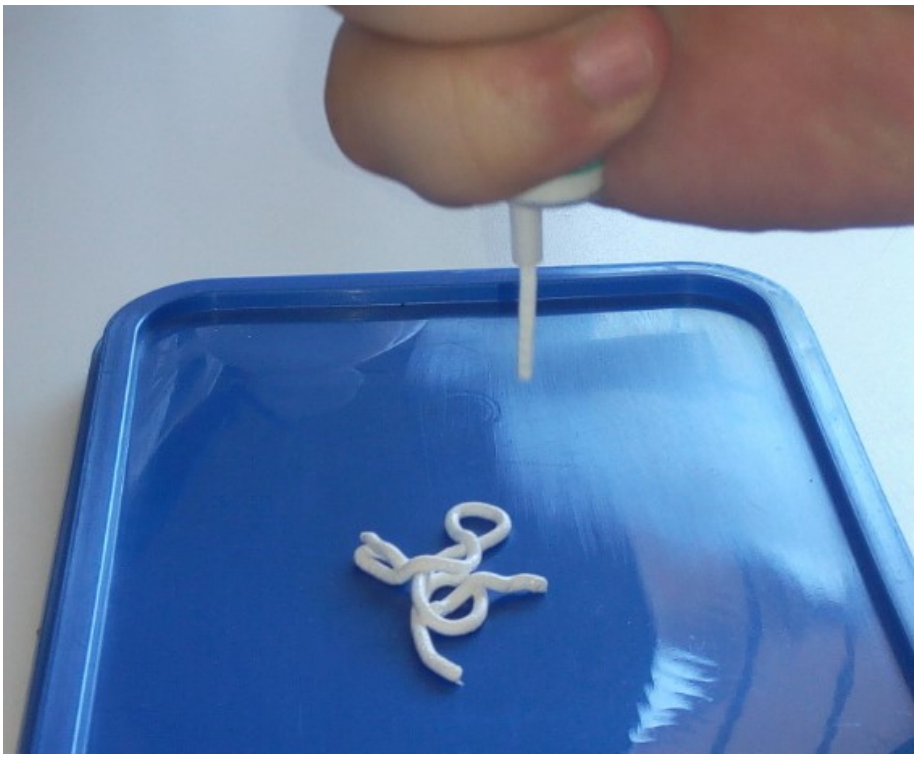

Figure 14: Injectability testing, paste runs out of the syringe hub without phase separation.

The injectability of cement is an essential quality of an injectable CPC that is supposed to be used during surgery. This α-TCP cement proved to be completely injectable but due to lack of adequate instrumentation, only the qualitative evaluation was used. Delgado et al. quantified the injectability of the prepared cements (65). A cement comparable with the cement in this work by its particle size had the injectability of only 39,1 %. The authors suggested improving the injectability by adding egg albumen, which increased the injectability to 93,0 %. Shi et al. on the other hand, presented results with α-TCP cement being injectable from 79 % (66). The injectability increase was noticed by increasing the content of citric acid in the liquid phase. This approach improves injectability and shortens setting time, on the other hand, it reduces the compressive strength of such cement. These qualities must be therefore carefully balanced. Bohner et al. suggest improving the injectability by increasing liquid to powder ratio when paste in being prepared, using a finer powder of solid phase, and by shortening and widening cannulas (45).

5.4 Washout resistance

The qualitative washout resistance testing showed no signs of debris, color change, transparency, or turbidity in any of the testing solutions (PBS, Ringer's, Normal saline). The testing spheres remained compact throughout the testing which can support the great potential of the paste to be suitable for injection during surgery.

Figure 15: Washout resistance testing. 5 mm diameter balls immersed in normal saline, Ringer's, and phosphate buffer saline solutions. No sign of disintegration is apparent.

Sufficient washout resistance of α-TCP based cement is a prerequisite for a successful injectable cement. The fact that α-TCP based cement is generally capable of flawless washout resistance is supported by Takagi et al. (62). The washout resistance of different compositions of CPCs was examined. It was suggested that a 90% α-TCP cement has excellent washout resistance. A closely connected quality of the cement which is setting time was improved with a higher content of Na_2HPO_4 in the liquid phase. The cement setting times are an important cement feature and could be a further continuation for the cement presented in the current work. An ideal cement should have its initial setting time between 3 and 8 minutes and final setting time longer than 15 minutes (47). Experiments in this work were performed in a static fluid environment. On the other hand, Shi et al. examined the washout resistance in a dynamic-shaking fluid environment (66). The findings support the outcome that a pure paste made predominantly from α-TCP with the addition of $CaCO_3$ would disintegrate after 15 minutes. It was also suggested that a possible solution to this complication could be the addition of citric acid and sodium

alginate into the cement. The washout resistance capacity examination of the cement prepared in this work in a dynamic environment would be an interesting topic for further research.

5.5 Raman spectroscopy

Raman spectroscopy elucidated the qualitative transformation of α-TCP to calcium-deficient hydroxyapatite. The Raman spectra of pure cement block after one day of hardening showed a high degree of similarity to the spectrum of standard hydroxyapatite rather than to α-TCP. The correlation of peaks is most apparent at the highest peak, where the sample had its maximum of the signal at 959,78 cm^{-1}, the standard of HAP at 962,00 cm^{-1}, and α-TCP at 968,63 cm^{-1}. A considerable similarity can be observed also at minor peaks e.g., at 427 cm^{-1} or 588 cm^{-1}.

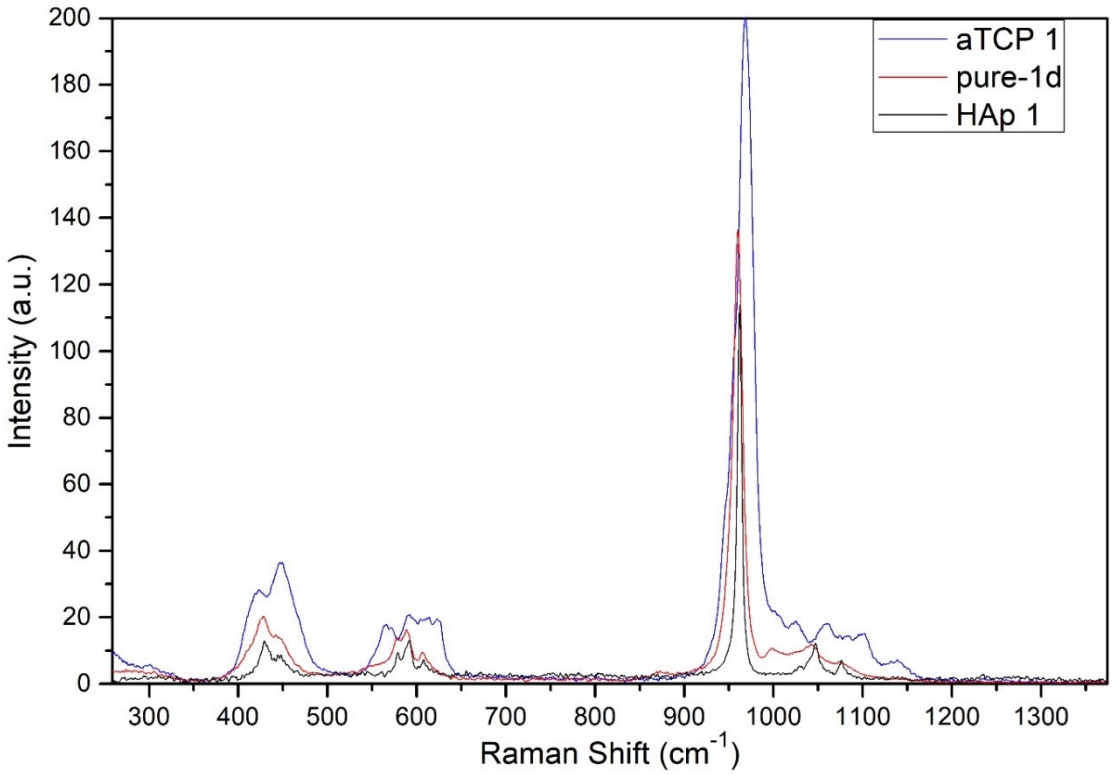

Figure 16: Raman spectra of a-TCP (blue), pure cement after one day of hardening (red), and standard of hydroxyapatite (black).

The spectra of these three samples correspond to the prediction found in the literature that after 24 hours of hardening, the majority of α-TCP would have transformed to calcium-deficient hydroxyapatite (67). The highest peak around 965 cm^{-1} is the phosphate band of symmetric P-O stretching, common to all three samples. Regions of 430 cm^{-1} and 1050 cm^{-1} are characteristic for P-O bending and anti-symmetric P-O stretching

respectively (67). The absence of splitting of the peak at 940 cm^{-1} and 970 cm^{-1}, characteristic for β-TCP, confirms the hypothesis that α-TCP was synthesized without a significant contribution of β-TCP (68). Ginebra et al. suggested that after 24 hours of hardening of α-TCP, the degree of conversion to calcium-deficient hydroxyapatite is cca 78 %, while full conversion occurs at 15 days (11). In addition, it was suggested that the compressive strength of the cement linearly correlates with the degree of conversion. The same results were also published by Fernández et al. (69). Current findings during this work are in agreement with the previous findings.

5.6 Compressive strength

Compressive strengths of pure and ibuprofen-loaded cements are shown in Figure 17. Pure cement exhibited significantly higher resistance to pressure than ibuprofen-loaded cement during the whole hardening process. More specifically, the highest average compressive strength was noticed at 9 days of hardening for pure cement (47,06 ± 7,50 MPa) and at 15 days for ibuprofen-loaded cement (3,72 ± 1,13 MPa). The exact values of compressive strength measurements and the standard deviations can be found in Table 1.

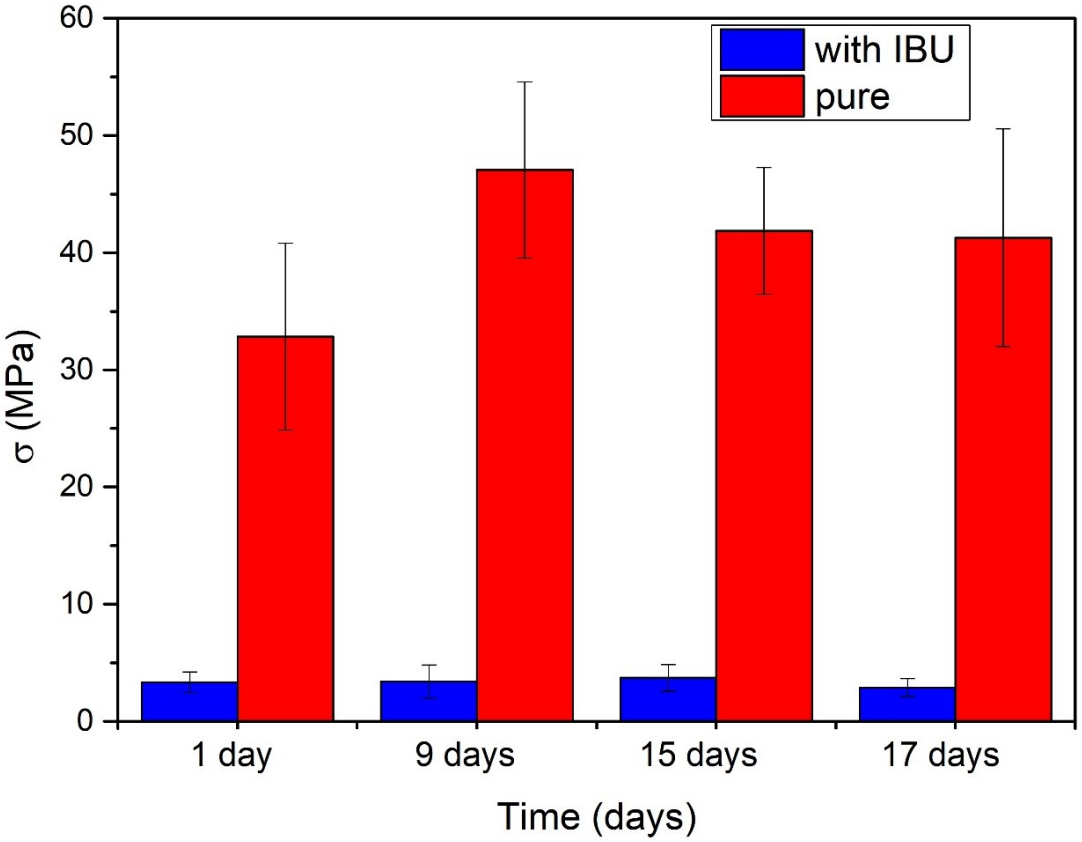

Figure 17: Graph depicting the relationship between the compressive strength of cement blocks and the time of hardening. Blue columns represent ibuprofen-loaded cement blocks and red columns represent pure cement blocks.

Days of hardening	Ibuprofen-loaded		Pure	
	σ (MPa)	SD	σ (MPa)	SD
1	3,3350	0,8844	32,8384	7,9699
9	3,4095	1,3957	47,0629	7,5031
15	3,7212	1,1338	41,8565	5,4125
17	2,8930	0,7821	41,2805	9,2825

Table 1: Values of compressive strength and standard deviations of ibuprofen-loaded and pure cement during hardening.

Even if the mean values of compressive strength for the pure cement decrease at 15 and 17 days of hardening, the decline is still in the standard deviation range. Thus, there is probably no degradation process occurring *in vitro* that would cause a gradual decline in compressive strength. Alexopoulou et al. noticed that the compressive strength of pure cement after 24 hours of testing was 27,4 ± 2,6 MPa (70), which is slightly less than the value observed in this work (32,84 ± 7,97 MPa) but within the boundaries of standard deviation. Takahashi et al. found the compressive strength of pure α-TCP cement to be

42 ± 4 MPa after 7 days of hardening (64). An analogous result (34,24 ± 3,02 MPa) for pure cement after 14 days of hardening was presented by Thürmer et al. (71). Since the compressive strength of the cortical bone of the human femur is 141,6 ± 15,91 MPa, the α-TCP based cement cannot be used for a load-bearing purpose when the full body weight would be applied. For purposes of substitution of a trabecular bone in various non-load-bearing applications, the compressive strength implies possible use. Compared to PMMA cements that are now commercially available for surgical purposes namely vertebroplasty, the compressive strength of α-TCP based cement is half of the PMMA (72).

An enormous 12,65-fold decrease in maximal compressive strength of ibuprofen-loaded cement compared to the pure one is the most noticeable finding of this experiment. This phenomenon, according to results in part 5.2. Hardening of cements and X-ray diffraction, cannot be explained by the conversion of α-TCP to calcium-deficient hydroxyapatite in ibuprofen-loaded samples not taking place. Although the mechanical properties of calcium phosphate cements generally correlate with the microstructure of the cement, in this work this discrepancy could not be resolved by SEM pictures (results shown in the next chapter). The lowest compressive strength of trabecular bone is around 2 MPa, which is less than the compressive strength of the ibuprofen-loaded cement, yet these results can be potentially improved. This could be achieved either by adding the drug in the liquid phase or by the addition of drug which is incorporated in polymer particles (71) (73). Otsuka et al. used a different approach in drug incorporation; cement was (after setting) immersed in an indomethacin solution which lead to the soaking of cement blocks with the active substance (74). This approach ensured sufficient compressive strength of 25,8 ± 2,26 MPa but excludes the possibility to inject the cement paste.

5.7 Scanning electron microscopy

The microstructure of the outer (Figures 18 and 19) and the inner surface (Figures 20 and 21) of the pure and outer (Figures 22 and 23) and the inner surface (Figures 24 and 25) of ibuprofen-loaded cement cylinders after 9 days of hardening showed no significant differences between samples. These findings cannot explain the disparity in the mechanical properties of the two samples. Albeit the fact that compressive strength of pure cement is 13,8 times higher than the ibuprofen-loaded cement after 9 days of hardening, the microstructure elements that are responsible for high mechanical strength i.e. interlocking planes and needles of calcium-deficient hydroxyapatite, are slightly more visible in the ibuprofen-loaded samples. This difference is mostly noticed on the outer surface of cement blocks, wherein the microstructure of pure cement is significantly less intertangled.

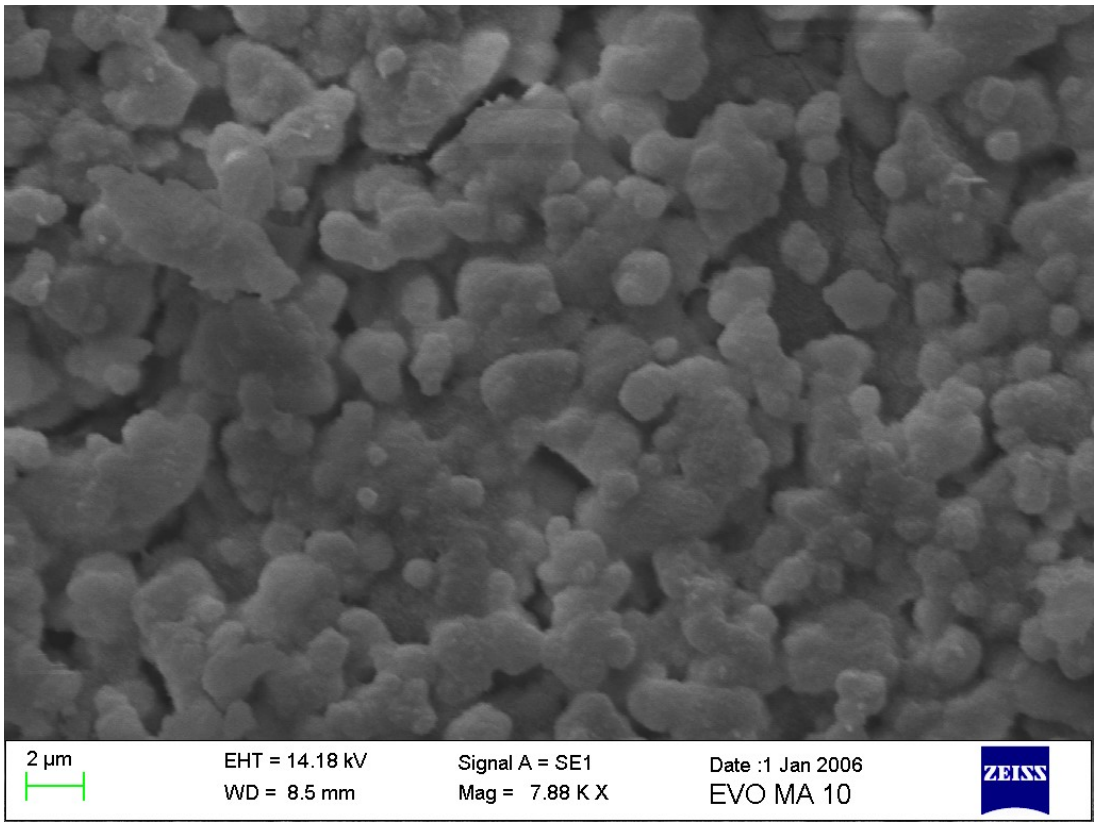

Figure 18: Outer surface of pure cement block after 9 days of hardening.

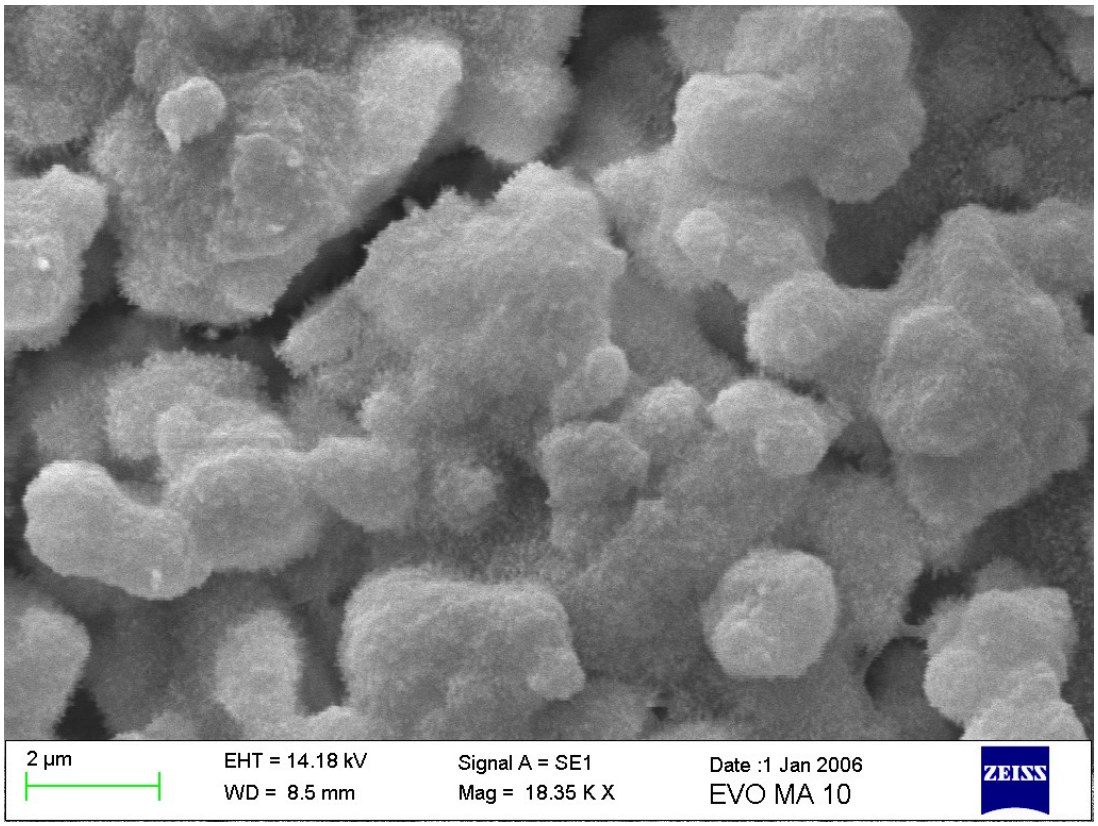

Figure 19: Outer surface of pure cement block after 9 days of hardening. Small needles are pointing out of the surface are visible.

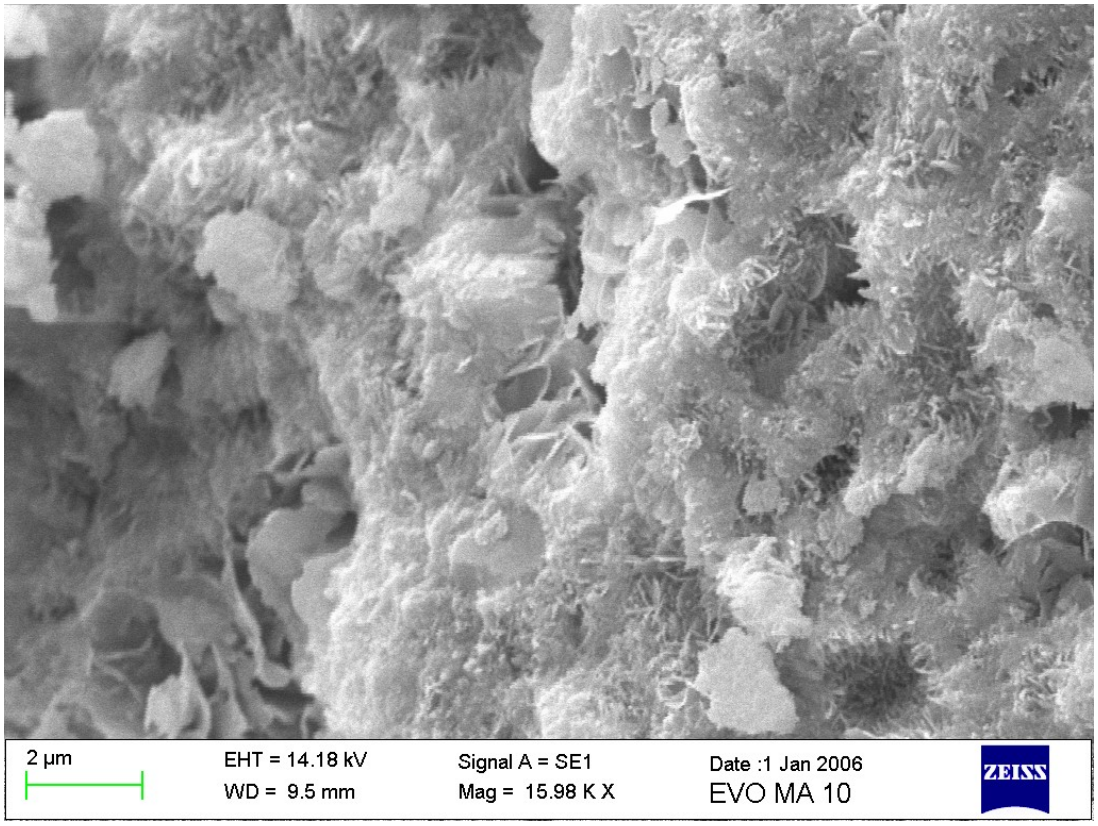

Figure 20: Inner surface of pure cement after compressive strength testing after 9 days of hardening. Precipitated planes and needles of calcium-deficient hydroxyapatite are apparent.

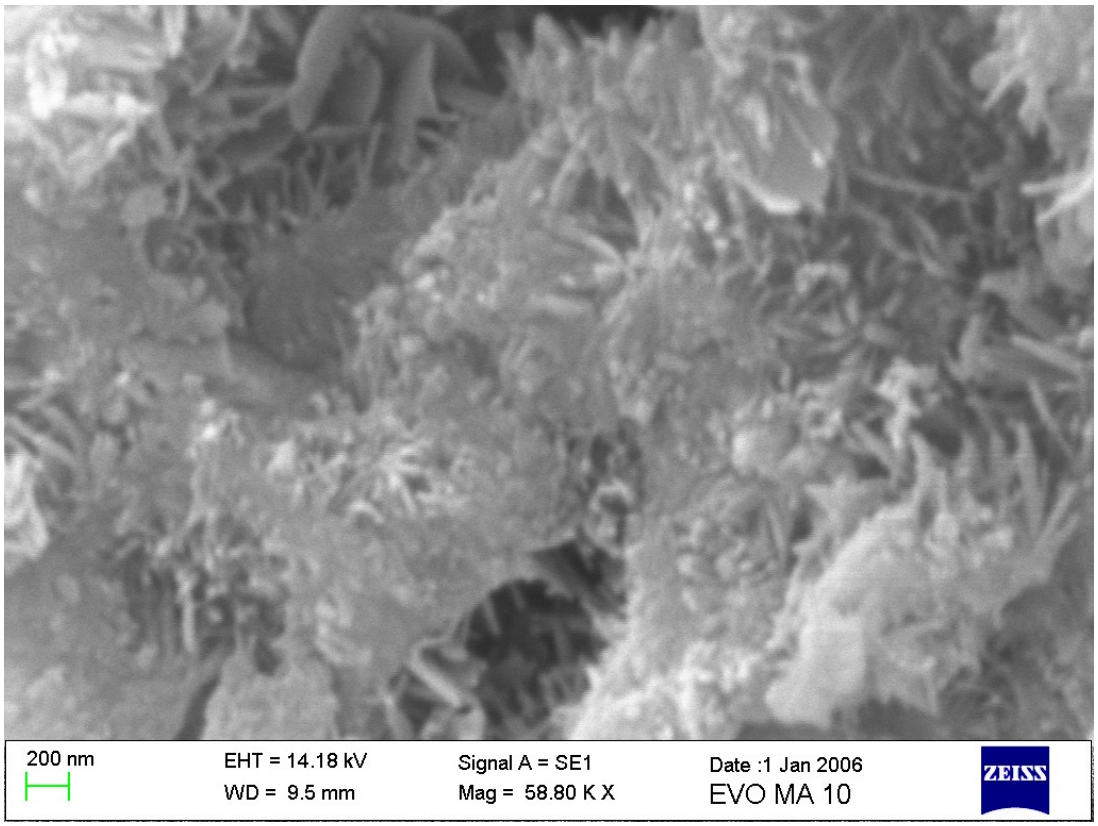

Figure 21: Close-up of the inner surface of pure cement after compressive strength testing after 9 days of hardening. Precipitated planes and needles of calcium-deficient hydroxyapatite are interlocked.

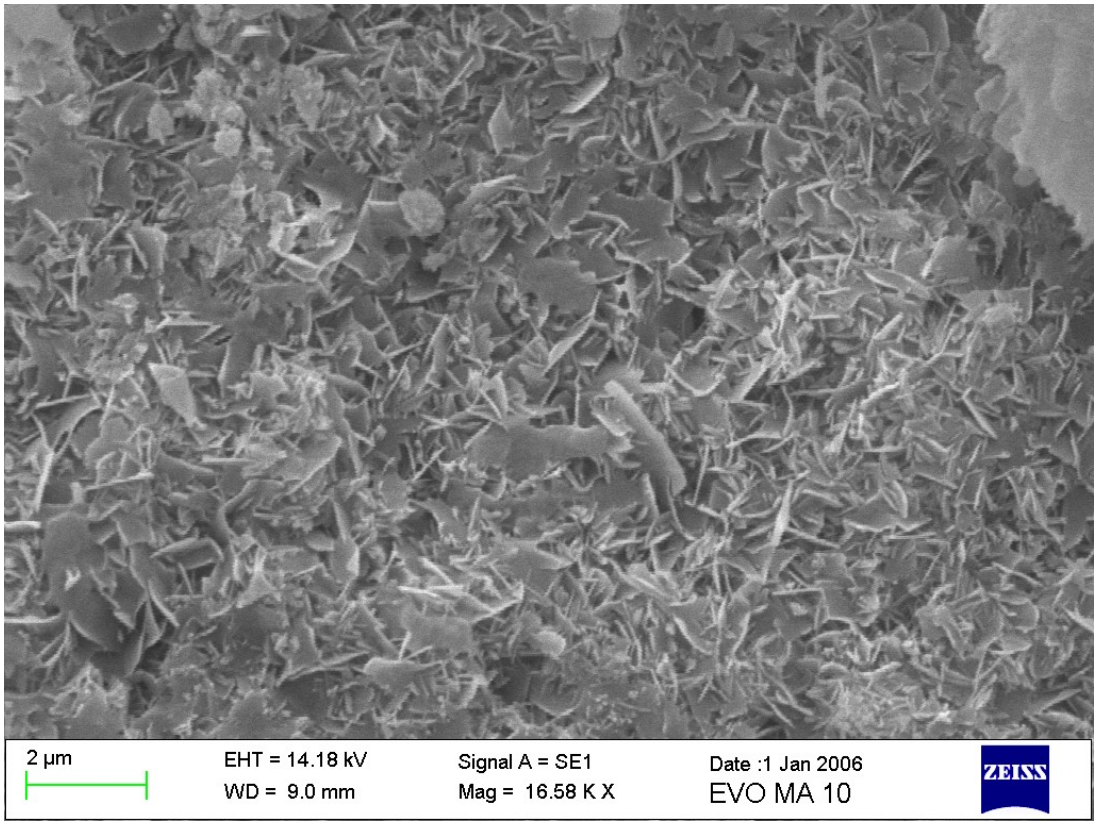

Figure 22: Outer surface of ibuprofen- loaded cement after 9 days of hardening. Planes of calcium-deficient hydroxyapatite are evident.

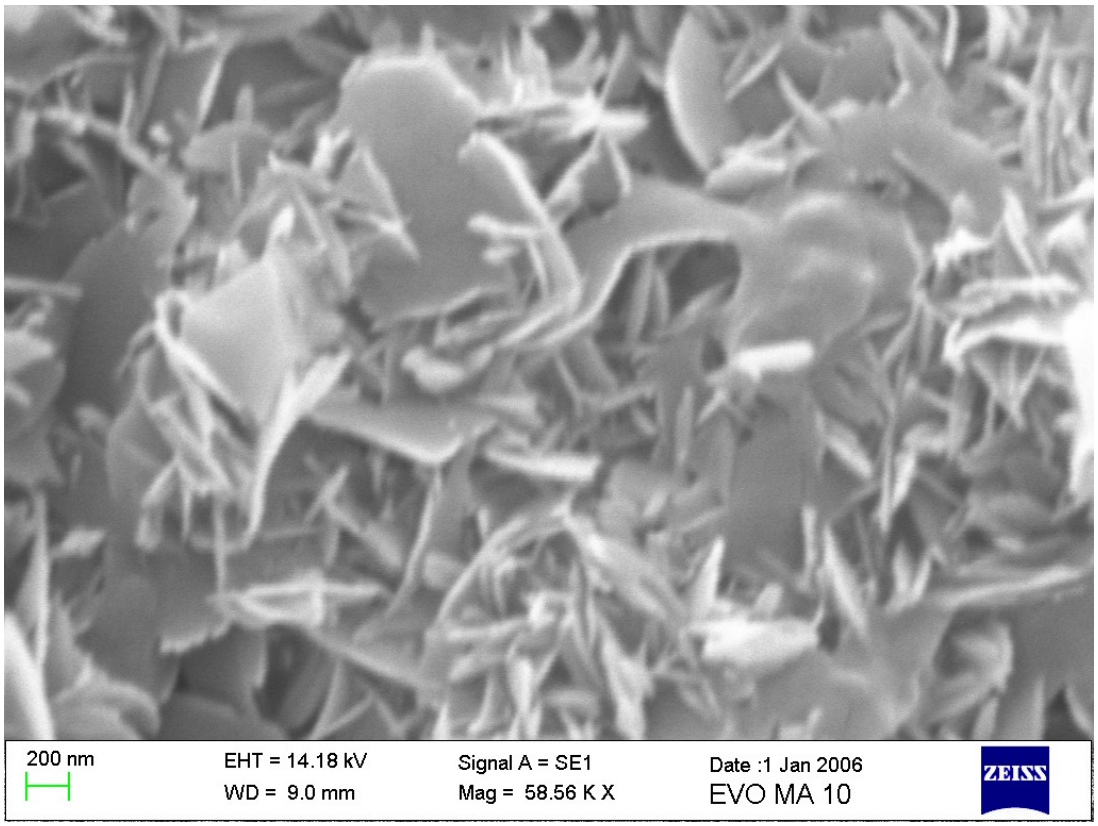

Figure 23: Close-up of the outer surface of ibuprofen-loaded cement after 9 days of hardening. Interwoven planes are more visible than in pure cement.

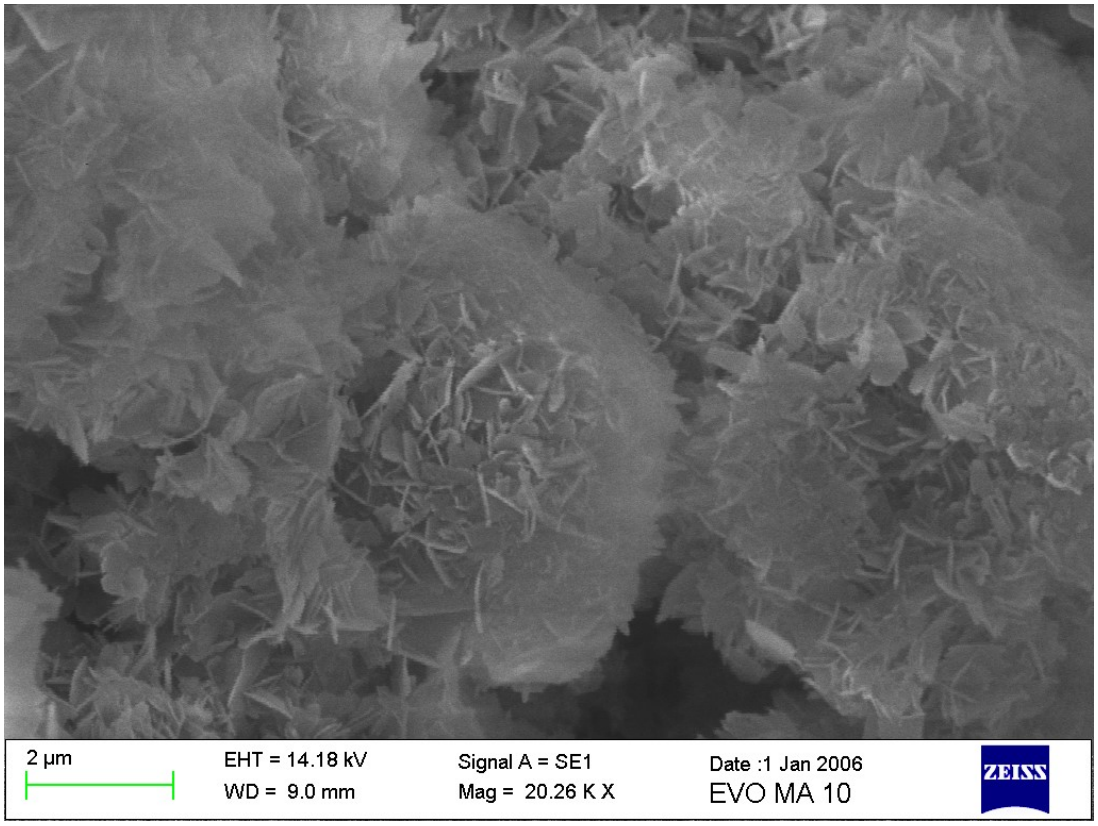

Figure 24: The inner surface of ibuprofen-loaded cement after compressive strength testing after 9 days of hardening. The inner surface resembles the outer more than in the samples of pure cement.

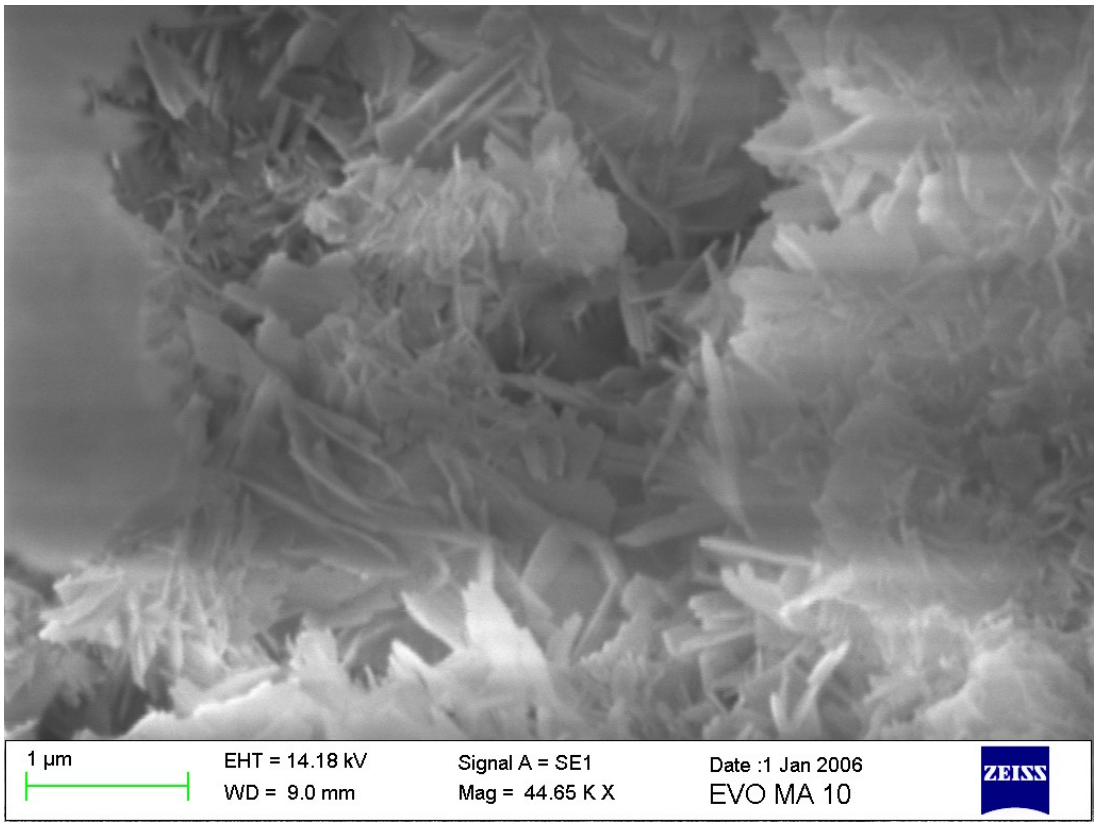

Figure 25: Close-up of the inner surface of ibuprofen-loaded cement after compressive strength testing after 9 days of hardening. Planes and needles are clearly observable.

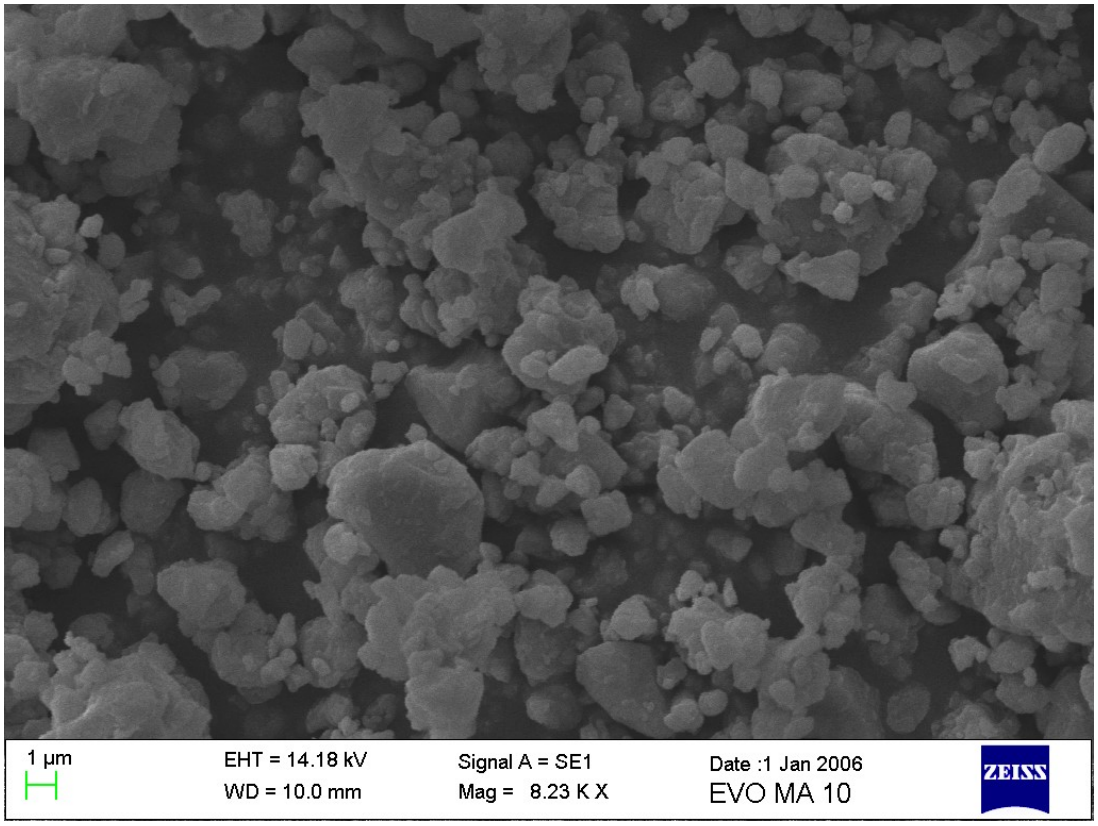

Figure 26: Grains of α-TCP powder after the milling process. The small diameter of particles increases the reactivity of α-TCP.

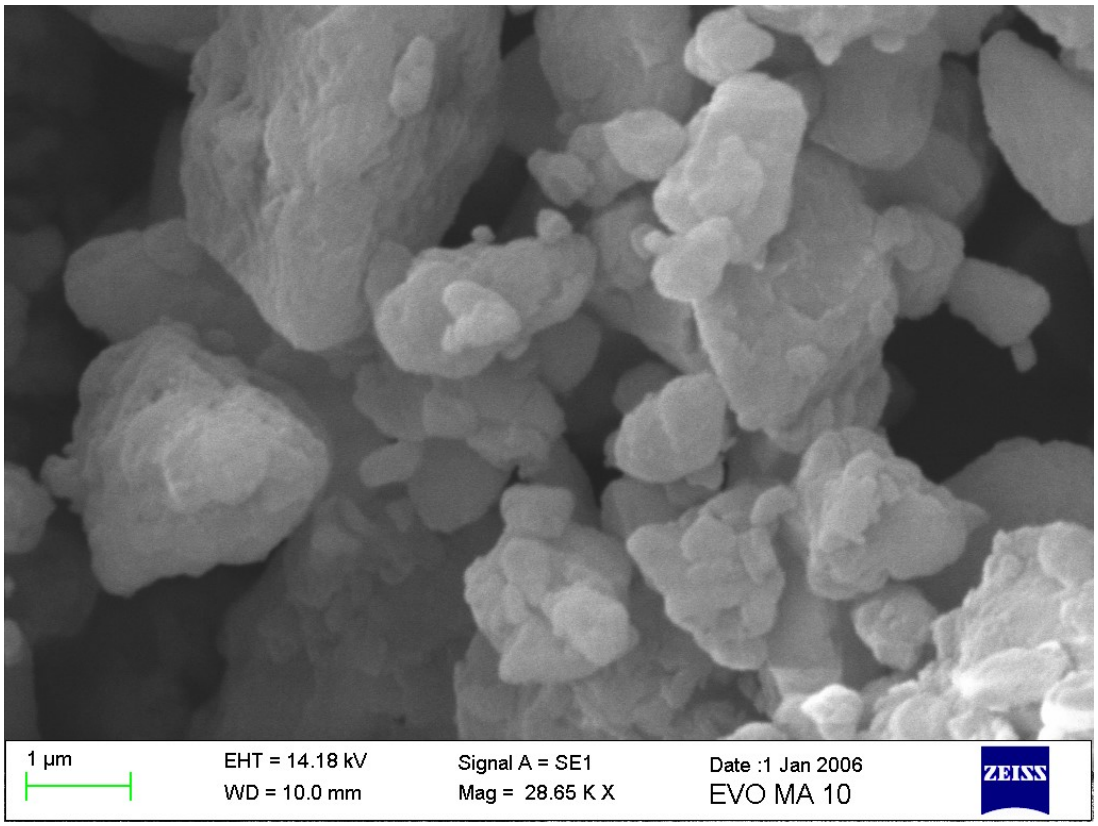

Figure 27: Close-up of α-TCP grains.

Images of the α-TCP powder (Figures 26 and 27) that was used as the solid-phase in all hydration reactions were obtained to confirm the high efficacy of the milling process. As expected, no signs of needles or planes of calcium-deficient hydroxyapatite were present. SEM image of α-TCP grain (Figure 27) shows comparable or even finer milling than what presented by Durucan et al. (75). The preparation was almost similar which leads to the analogous appearance of α-TCP particles with a diameter of 3,3 µm or less. Durucan et al. also presented SEM images of pure cement formed after only 18 hours of hardening at 37°C. The presented images showed crystals of calcium-deficient hydroxyapatite in the form of planes and needles similar to those on the inner surface of pure cement (Figure 21). Morejón-Alonso et al. presented SEM images of pure cements' inner and outer surface after 7 days of hardening (76). Interestingly, they found a high similarity between the inner and the outer surface structures. These findings are not in accordance with the results of this work since a distinct difference between the inner surface (Figure 20) and the outer surface (Figure 19) is apparent. Absence of a plate-like structure on the outer surface (Figure 18 and Figure 19) with only small needle-like formations might be due to the relatively high volume of PBS in which

the cylinders were immersed, hence the supersaturation on the surface leading to crystal growth was present to a lesser extent.

To the best of our knowledge, there is no previous study presenting SEM images of ibuprofen-loaded cement. Thus, no direct comparison can be conducted. Any potential indirect comparison is possible only with drug-loaded cements which are using different precursors or the drug is loaded into cement blocks after their hardening. A relatively comparable study conducted by Sugo et al. shows pictures of cement made from α-TCP, TeCP, DCPD, and hydroxyapatite with vancomycin and gentamicin added to the cement paste (77). The SEM images showed that the addition of vancomycin causes blockage of crystal growth whereas the addition of gentamicin is relatively inert. Although this hypothesis is supported by data of compressive strength and median pore diameter, the microstructure evaluated from pictures alone does not seem to be significantly more tortuous in gentamicin samples. Another related study is by Noukrati et al. where sodium fusidate was loaded in cement made from calcium carbonate and DCPD (78). The structure of hardened cement consisted of mainly small needles with no significant difference between pure and fusidate-loaded cement. Plate-like structures, like those which are present in Figures 22, 23, 24, and 25 are absent in the abovementioned work. This is probably not due to a smaller diameter of particles but rather due to a different end product – brushite.

The difference between the inner surface structure of pure and ibuprofen-loaded cement in this work is insignificant. Distinct plates and needles interlock in both cases. This finding is contrary to the data from compressive strength testing, where the ibuprofen-loaded cement's failure load was after 9 days of hardening 13,8 times lower than of pure cement. This disparity cannot be elucidated by microstructural characteristics visible form SEM.

5.8 Dissolution testing

In order to investigate the ibuprofen release from the cement, dissolution testing was performed. The concentrations were measured spectrophotometrically with a prior measurement of a calibration curve for both wavelengths i.e. at 264,3 nm and 272,8 nm. These calibration curves are depicted in Figure 28. The R^2 was 0,9994 and 0,9993 respectively, which indicates a very reliable calibration. The testing of dissolution confirmed the hypothesis of a prolonged-release (40) as can be noticed in Figure 29

for 264,3 nm and in Figure 30 for 272,8 nm. Data obtained from both wavelengths proved similar release of ibuprofen from the cement to PBS after 21 days (84,6 % ± 9,51 % and 84,30 % ± 9,82 % at 264,3 and 272,8 nm respectively).

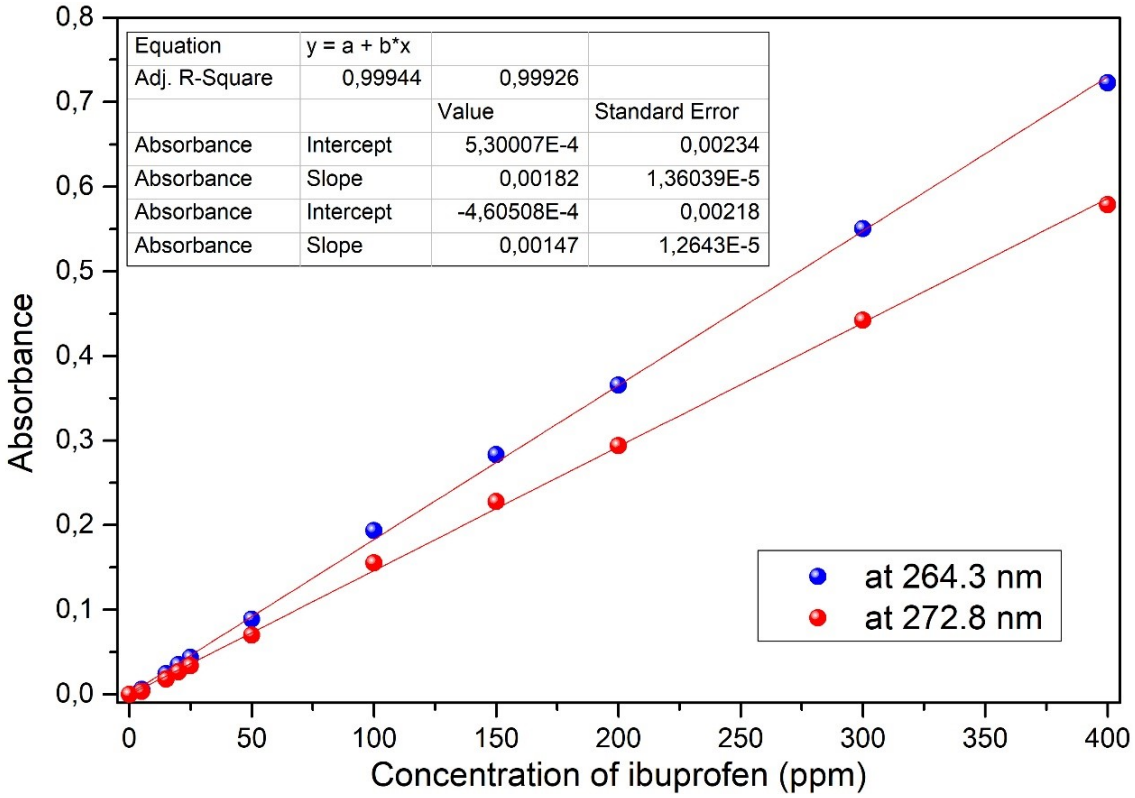

Figure 28: Graph depicting calibration curves for concentrations. Blue dots represent values measured for 264,3 while red dots represent values measured at 272,8 nm. The values of R-square is for 264,3 and 272,8 nm respectively. The value of intercept corresponds to the ''a'' in the general equation and slope to the ''b''. The values of slope and intercept for 264,3 nm are the upper two, while for 272,8 nm are valid the two lower ones.

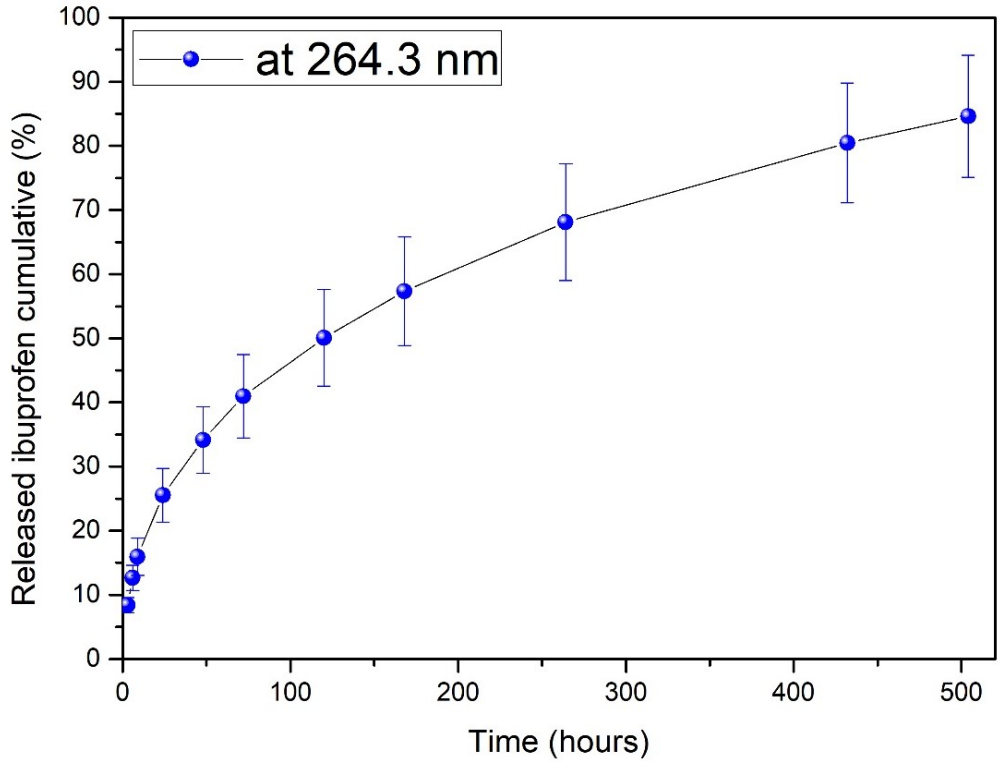

Figure 29: Graph depicting dissolution of ibuprofen from tablets made of cement paste. Cumulative % of ibuprofen released versus time in hours. Samples were measured at 264,3 nm. Error bars represent the standard deviation between four sample tablets.

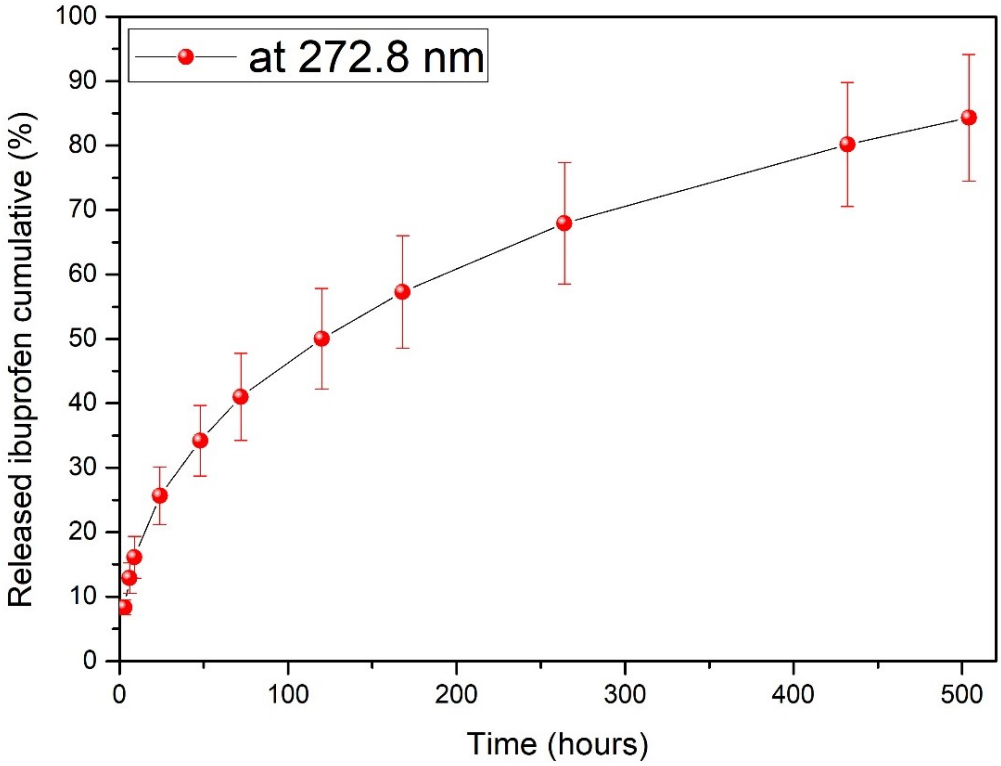

Figure 30: Graph depicting dissolution of ibuprofen from tablets made of cement paste. Cumulative % of ibuprofen released versus time in hours. Samples were measured at 272,8 nm. Error bars represent the standard deviation between four sample tablets.

After adjustment of the x-axis to $\sqrt{t}$ according to Higuchi's law, the R^2 of 4 tablets' average values for each wavelength was 0,9866 and 0,9862 respectively. Korsmeyer-Peppas model showed results of n= 0,4404; K= 6,0900 with R^2= 0,9991 and n= 0,4376; K= 6,1718 with R^2= 0,9991 for wavelengths 264,3 nm and 272,8 nm respectively. The dissolution profile of ibuprofen followed the Higuchi's law as predicted by Ginebra et al. to an even greater proportion of dissolved ibuprofen (79). More specifically, Ginebra et al. described the dissolution following the Higuchi's law up to 60 % of released ibuprofen while in this experiment the dissolution followed it throughout the whole course at a sufficient R^2. Korsmeyer-Peppas' kinetic model showed for this experiment expected n-values for a non-resorbable matrix system. The values exactly correspond to those calculated for a Fick related diffusion from non-swellable cylindrical models by Ritger and Peppas (80). The fact that the dissolution of ibuprofen took over 430 hours to reach 80 % of drug dissolved indicates some form of interaction between cement and ibuprofen of very tortuous internal structure limiting the speed. In a study performed by Fullana et al. with different CPC where ibuprofen-loaded cement was a control sample, the full dissolution took only 48 hours, while the use of retarding agent prolonged the dissolution up to 45 days. This article also confirms the Fick type of diffusion and validity of Higuchi's law throughout the dissolution of ibuprofen (73). Another study used 2 % of ibuprofen addition to α-TCP cement as a control for gypsum enriched cement. Their dissolution profile reached 80 % after cca 200 hours which is more than two times faster in comparison with this work (70).

6. Conclusion

Since their first discovery, almost two centuries ago, calcium phosphate cements underwent a long journey as it concerns their synthesis, characterization, and potential uses. This work is one small addition at the mosaic of knowledge that could likely contribute to a better understanding of this extraordinary material.

The calcium phosphate cement, based on α-TCP was the main focus of this thesis. The synthesis of α-TCP from calcium carbonate and calcium pyrophosphate was a very effective method for obtaining material of desired quality with a negligible contribution of impurities. Cement paste prepared by mixing of α-TCP with liquid phase proved to possess essential characteristics that are appropriate for surgical application – injectability and washout resistance. As a simulation of the physiological environment, the cement blocks hardened in a PBS solution. The course of the transition of α-TCP was monitored by X-ray diffraction. Obtained data showed that, after one day, a significant portion of α-TCP underwent hydration reaction to calcium-deficient hydroxyapatite. This process was found to be common for pure and ibuprofen-loaded cement and is still apparent until day 17 of hardening. A parallel experiment, investigating mechanical properties of the cement blocks, both pure and ibuprofen-loaded, throughout the hardening, showed a promising compressive strength of pure cement after 9 days of hardening. Moreover, the obtained values were sufficient already after 1 day of hardening for non-load-bearing applications. Ibuprofen-loaded cement, despite a similar course of hydration reaction, exhibited very poor compressive strength. Few suggestions about the modifications of experiment design were made to further investigate this phenomenon. Raman spectroscopy was used to shed light on the transformation of α-TCP to calcium-deficient hydroxyapatite. The results showed the majority of α-TCP is transformed to calcium-deficient hydroxyapatite after 24 hours of hardening. A deeper observation of the microstructure of the cements by SEM microscopy was performed. SEM images revealed crystals of calcium-deficient hydroxyapatite and fine powder of α-TCP. In addition, the dissolution profile of ibuprofen from cement tablets was investigated. Calcium phosphate cement proved to be a matrix capable of sustained drug release according to Higuchi's law.

7. Bibliography

1. **Dorozhkin, S. V., Epple, M.** Biological and Medical Significance of Calcium Phosphates. *Angewandte chemie international edition.* 2002, Vol. 41, 17, pp. 3130-3146.

2. **Brown, W. E. and Chow, L. C.** A new calcium phosphate setting cement. *Journal of Dental Research.* 1983, 62, p. 672.

3. **Schrödter, K., Bettermann, G., Staffel, T., Wahl, F., Klein, T., Hofmann, T.** Phosphoric acid and phosphates. *Ullmann's encyclopedia of industrial chemistry.* 2008.

4. **Fernández, E., Gil, F. J., Ginebra, M. J., Driessens, F. C. M., Planell, J. A.** Calcium phoshate bone cements for clinical applications, Part I: Solution chemistry. *Journal of materials science: Materials in medicine.* 1999, Vol. 10, 3, pp. 169-176.

5. **Bohner, M.** Calcium orthophosphates in medicine: from ceramics to calcium phosphate cements. *Injury.* 2000, Vol. 31, pp. 37-47.

6. **National Center for Biotechnology Information. PubChem database.** *Calcium Phosphate.*

7. **Carrodeguas, R. G., De Aza, S.** α-Tricalcium phosphate: Synthesis, properties and biomedical applications. *Acta biomaterialia.* 2011, Vol. 7, 10, pp. 3536-3546.

8. **Buerger, M. J.** The role of temperature in mineralogy. *Am Miner.* 33, 1948, Vols. 3-4, pp. 101-21.

9. **Chen, F., Ma, X., Yu, Y., Liu, C.** Calcium Phosphate Bone Cements: Their Development and Clinical Application. [book auth.] He H. Liu C. *Developments and Applications of Calcium Phosphate Bone Cements.* Singapore : Springer Nature, 2018, pp. 1-40.

10. **Vallet-Regí, M., Gonzáles-Calbet, J. M.** Calcium phopshates as substitution of bone tissues. *Progress in Solid State Chemistry.* 2004, Vol. 32, pp. 1-31.

11. **Ginebra, M. P., Fernández, E., De Maeyer, E. A. P., Verbeeck, R. M. H., Boltong, M. G., Ginebra, J., Driessens, F. C. M., Planell, J. A.** Setting Reaction and Hardening of an Apatitic Calcium Phosphate Cement. *Journal of Dental Research.* 1997, Vol. 76, 4.

12. **Čihák, R., Grim, M., Fejfar, O.** *Anatomie 1.* Prague : Grada, 2013. pp. 61-75. ISBN 978-80-247-3817-8.

13. **Dylevský, I.** *Funkční anatomie.* Prague : Grada, 2009. pp. 71-88. ISBN 978-80-247-3240-4.

14. **Farokhi, M., Mottaghitalab, F., Samani, S., Shokrgozar, M. A., Kundu, S. C., Reis, R. L., Fattahi, Y., Kaplan, D. L.** Silk fibroin/hydroxyapatite composites for bone tissue engineering. *Biotechnology advances.* 2018, Vol. 36, 1, pp. 68-91.

15. **Whedon, G. D., Heaney, R. P.** Bone. *Encyclopædia Britannica.* [Online] March 19, 2019. [Cited: November 12, 2019.] https://www.britannica.com/science/bone-anatomy.

16. **Troy, E.** Tension, compression, shear and torsion. *Strengthminded.* [Online] February 16, 2019. [Cited: May 11, 2020.] https://www.strengthminded.com/tension-compression-shear-and-torsion/.

17. **Havaldar, R., Pilli, S. C., Putti, B. B.** Insights into the effects of tensile and compressive loadings on human femur bone. *Advanced Biomedical Research.* 2014, Vol. 3, 101.

18. **Hannink, G., Arts, J. J. C.** Bioresorbability, porosity and mechanical strength of bone substitutes: What is optimal for bone regeneration? *Injury.* 2011, Vol. 42, pp. 22-25.

19. **Marsell, R., Einhorn, T. A.** The biology of fracture healing. *Injury.* 2011, Vol. 42, 6, pp. 551-555.

20. **Granero-Moltó, F., Weis, J. A., Miga, M. I., Landis, B., Myers, T. J., O'Rear, L.** Regenerative Effects of Transplanted Mesenchymal Stem Cells in Fracture Healing. *Stem Cells.* 2009, Vol. 27, 8, pp. 1887-1898.

21. **McKibbin, B.** The Biology of Fracture healing in Long Bones. *Journal of bone and joint surgery.* 60-B, 1978, Vol. 2, pp. 150-162.

22. **Barnes, G.L., Kostenuik, P.J., Gerstenfeld, L.C.** Growth factor regulation of fracture. *Journal of bone and mineral research.* 1999, Vol. 14, 11, pp. 1805-1815.

23. **Mousa, W. F., Kobayashi, M., Shinzato, S., Kamimura, M., Neo, M., Yoshihara, S., Nakamura, T.** Biological and mechanical properties of PMMA-based bioactive bone cements. *Biomaterials.* 2000, Vol. 21, 21, pp. 2137-2146.

24. **Ginebra, M. P.** Calcium phosphate bone cements. *Orthopaedic Bone Cements.* 2008, pp. 206-230.

25. **Lee, C.** The Mechanical Properties of PMMA Bone Cement. [book auth.] Malchau Breusch. *Well-Cemented Total Hip Anthroplasty.* Berlin Heidelberg : Springer, 2005, pp. 60-66.

26. **Ginebra, M. P.** Calcium phosphate bone cements. [book auth.] Sanjukta Deb. *Orthopaedic bone cements.* 1st. s.l. : Woodhead Publishing, 2008, pp. 206-224.

27. **Fernández, E., Gil, F. J., Ginebra, M. P., Driessens, F. C. M., Planell, J. A.** Calcium phosphate bone cements for clinical, Part II: Precipitate formation during setting reactions. *Journal of materinal science: Materials in medicine.* 10, 1999, pp. 177-183.

28. **TenHuisen, K., Kevor, S., Brown, P. W.** Formation of calcium-deficient hydroxyapatite from α-tricalcium phosphate. *Biomaterials.* 1998, Vol. 19, 23, pp. 2209-2217.

29. **Ginebra, M. P., Driessens, F. C. M., Planell, J. A.** Effect of the particle size on the micro and nanostructural features of a calcium phosphate cement: a kinetic analysis. *BIomaterials.* 2004, Vol. 25, 17, pp. 3453-3462.

30. **Andriotis, O., Katsamenis, O. L., Mouzakis, D. E., Bouropoulos, N.** Preparation and characterization of bioceramics produced from calcium phosphate cements. *Crystal research and technology.* 2010, Vol. 45, 3, pp. 239-243.

31. **LeGeros, R. Z.** Properties of osteoconductive biomaterials: Calcium phosphates. *Clinical orthopaedics and related research.* 2002, Vol. 395, pp. 81-98.

32. **Liu, C., Wang, W., Shen, W., Chen, T., Hu, L., Chen, Z.** Evaluation of the biocomatibility of a nonceramic hydroxyapatite. *Journal of Endodontics.* 1997, Vol. 23, 8, pp. 490-493.

33. **Wang, J., Liu, C.** Calcium phosphate composite cement. [book auth.] C., He, H. Liu. *Developments and applications of calcium phosphate bone cements.* Hong Kong : Springer, 2018, pp. 187-221.

34. **Bohner, M.** Silicon-substituted calcium phosphates - A critical view. *Biomaterials.* 2009, Vol. 30, 32, pp. 6403-6406.

35. **Vallet-Regí, M., Arcos, D.** Silicon substitued hydroxyapatites. A method to upgrade calcium phopshate based implants. *Journal of materials chemistry.* 2005, Vol. 15, 15, pp. 1509-1516.

36. **Sadiasa, A., Sarkar, S. K., Franco, R. K., Min, Y. K., Lee, B. T.** Bioactive glass incorporation in calcium phosphate cement-based injectable bone substitute for improved in vitro biocompatibility and in vivo bone regeneration. *Journal of biomaterials applications.* 2013, Vol. 28, 5, pp. 739-756.

37. **Laskus, A., Kolmas, J.** Ionic substitutions in non-apatitic calcium phosphates. *International journal of molecular sciences.* 2017, Vol. 18, 12, pp. 2542-2563.

38. **Seehra, S. S., Gupta, S., Kumar, S.** Rapid setting magnesium phosphate cement for quick repair of concrete pavements - characterisation and durability aspects. *Cement and concrete research.* 1993, Vol. 23, 2, pp. 254-266.

39. **Wu, F., Wei, J., Guo, H., Chen, F., Hong, H., Liu, C.** Self-setting bioactive calcium–magnesium phosphate cement with high strength and degradability for bone regeneration. *Acta biomaterialia.* 2008, Vol. 4, 6, pp. 1873-1884.

40. **Ginebra, M. P., Traykova, T., Planell, J. A.** Calcium phopshate cements: Competitive drug carriers for the musculoskeletal system? *Bimaterials.* 2006, Vol. 27, 10, pp. 2171-2177.

41. **Kisanuki, O., Yajima, H., Umeda, T., Takakura, Y.** Experimental study of calcium phosphate cement impregnated with dideoxy-kanamycin B. *Journal of orthopaedic science.* 2007, Vol. 12, 3.

42. **Ginebra, M. P., Canal, C., Espanol, M., Pastorino, D., Montufar, E. B.** Calcium phopshate cements as drug delivery materials. *Advanced drug delivery reviews.* 2012, Vol. 64, pp. 1090-1110.

43. **Ratier, A., Freche, M., Lacout, J., Rodriguez, F.** Behaviour of an injectable calcium phopshate cement with added tetracycline. *International journal of pharmaceutics.* 2004, Vol. 274, 1-2.

44. **Hesaraki, S., Nemati, R.** Cephalexin-loaded injectable macroporous calcium phosphate bone cements. *Journal of biomedical materials research part B: applied biomaterials.* 2009, Vol. 89B, 2.

45. **Bohner, M., Baroud, G.** Injectability of calcium phosphate pastes. *Biomaterials.* 2005, Vol. 26, 13, pp. 1553-1563.

46. **Khairoun, I., Boltong, M. G., Driessens, F. C. M., Planell, J. A.** Some factors cotrolling injectability of calcium phoshate bone cements. *Journal of materials science: Materials in medicine.* 1998, Vol. 9, pp. 425-428.

47. **O'Hara, R., Buchanan, F., Dunne, N.** Injectable calcium phosphate cements for spinal repair. *Biomaterials for bone regeneration.* 2014, pp. 26-61.

48. **Olubiyi, O. I., Lu, F-K., Calligaris, D., Jolesz, F. A., Agar, N. Y.** Advances in molecular imaging for surgery. *Image-guided neurosurgery.* 2015, pp. 407-439.

49. **Princeton instruments.** Raman spectroscopy basics. *Princeton Instruments.* [Online] [Cited: January 5, 2019.] http://web.pdx.edu/~larosaa/Applied_Optics_464-564/Projects_Optics/Raman_Spectrocopy/Raman_Spectroscopy_Basics_PRINCETON-INSTRUMENTS.pdf.

50. **Horiba.** Raman data and analysis. *horiba.com.* [Online] [Cited: January 5, 2019.] https://static.horiba.com/fileadmin/Horiba/Technology/Measurement_Techniques/Molecular_Spectroscopy/Raman_Spectroscopy/Raman_Academy/Raman_Tutorial/Raman_bands.pdf.

51. **Bannerman, A., Williams, R. L., Cox, S. C., Grover, L. M.** Visialising phase change in brushite-based calcium phosphae ceramic. *Scientific reports.* 6, 2016, Vol. 1.

52. **Ameh, E. S.** A review of basic crystallography and x-ray diffration applications. *The international journal of advanced manufacturing technology.* 2019.

53. **Das, R., Ali, E., Hamid, S. B. A.** Current applicatons of x-ray powder diffraction - a review. *Reviews on advanced materials science.* 2014, Vol. 38, 2, pp. 95-109.

54. **Sharma, R., Bisen, D. P., Shukla, U., Sharma, B. G.** X-ray diffraction: a powerful method of characterizing nanomaterials. *Recent research in science and technology.* 2012, Vol. 4, 8, pp. 77-79.

55. **Hofer, K. E.** Materials testing. *Encyclopaedia brittanica.* [Online] June 6, 2018. [Cited: January 14, 2020.] https://www.britannica.com/technology/materials-testing.

56. **Bruschi, M. L.** *Strategies to modify the drug release from pharmaceutical systems.* s.l. : Woohdhead publishing series in biomedicine, 2015. p. 37. ISBN 978-0-08-100092-2.

57. **Uddin, R., Saffoon, N., Sutradhar, K. B.** Dissolution and dissolution apparatus: A review. *International journal of current biomedical and pharmaceutical research.* 2011, Vol. 1, 4, pp. 201-207.

58. **Erweka.** Dissolution on-/offline system with UV/VIS. *Erweka.* [Online] Erweka, January 1, 2019. [Cited: January 19, 2019.] https://www.erweka.com/products/dissolution-testers/dissolution-on-offline-system/item/dissolution-on-offline-system-uv-vis.html.

59. **De Caro, C. A.** *UV/VIS spectrophotometry - fundamentals and applications.* [Document] s.l. : Mettler-Toledo International, 2015.

60. **Klimeš, J., Sochor, J., Mokrý, M., Kastner, P., Pilařová, P.** *Kontrolně-analytické hodnocení léčiv lékopisnými metodami.* Hradec Králové : Jiří Klimeš, Farmaceutická fakulta Unverzity Karlovy, 2015. pp. 15-17. ISBN 978-80-260-8175-3.

61. **Ul-Hamid, A.** *A Beginners' guide to sanning electron microscopy.* Dhahran : Springer, 2018. ISBN 978-3-319-98481-0.

62. **Takagi, S., Chow, L. C., Hirayama, S., Sugawara, A.** Premixed calcium-phopshate cement pastes. *Journal of biomedical materials research.* 2003, Vol. 67B, 2, pp. 689-696.

63. **Cardoso, H. A. I., Motisuke, M., Zavaglia, C. A. C.** The influence of three additives on the setting reaction kinetics and mechanical strength evolution of [alpha]-tricalcium phosphate cements. *Key engineering materials.* 2012, Vols. 393-394, pp. 397-402.

64. **Takahashi, K., Fujishiro, Y., Yin, S., Sato, T.** Preparation and compressive strength of α-tricalcium phosphate based cement dispersed with ceramic particles. *Ceramics international.* 2004, Vol. 30, 2, pp. 199-203.

65. **Delgado, J. A., Harr, I., Almirall, A., del Valle, S., Planell, J. A., Ginebra, M. P.** Injectability of a macroporous calcium phosphate cement. *Key engineering materials.* 2005, Vols. 284-286, pp. 167-160.

66. **Shi, H., Zhang, W., Liu, X., Zheng, S., Yu, T., Zhou, C.** Synergistic effect of citric acid - sodium alginate on physicochemical properties of α-tricalcium phosphate bone cement. *Ceramics international.* 2019, Vol. 45, pp. 2146-2152.

67. **Kolmas, J., Kaflak, A., ZIma, A., Ślósarczyk, A.** Alpha-tricalcium phosphate synthesized by two different routes: Structural and spectroscopic characterization. *Ceramics international.* 2015, Vol. 41, 4, pp. 5727-5733.

68. **Jillavenkatesa, A., Condrate, R. A.** The infrared and Raman spectra of ß-and α-tricalcium phosphate (Ca3(PO4)2). *Spectroscopy letters: An international journal for rapid communication.* 1998, Vol. 31, 8, pp. 1619-1634.

69. **Fernández, E., Ginebra, M. P., Boltong, M. G., Driessens, F. C. M., Ginebra, J., De Maeyer, E. A. P., Verbeeck, R. M. H., Planell, J. A.,.** Kinetic study of the setting reaction of a calcium phosphate bone cement. *Journal of biomedical materials research.* 1996, Vol. 32, 3, pp. 367-374.

70. **Alexopoulou, M., Mystridou, E., Mouzakis, D., Zaoutsos, S., Fatouros, D., Bouropoulos, N.** Preparation, characterization and in-vitro assessment of ibuprofen loaded calcium phosphate/gypsum bone cement. *Crystal research and technology.* 2015, Vol. 51, 1, pp. 41-48.

71. **Thürmer, M. B., Diehl, C. E., Brum, F. J. B., dos Santos, L. A.** Development of dual.setting calcium phosphate cement using absrbable polymer. *Artificial organs.* 2013, Vol. 37, 11, pp. 992-997.

72. **Jasper, L. E., Deramond, H., Mathis, J. M., Belkoff, S. M.** Material properties of vrious cements for use with vertebroplasty. *Journal of materials science: Materials in medicine.* 2002, Vol. 13, 1, pp. 1-5.

73. **Girod Fullana, S., Ternet, H., Freche, M., Lacout, J. L., Rodriguez, F.** Controlled release properties and final macroporosity of a pectin microspheres-calcium phosphate composite bone cement. *Acta biomaterialia.* 2010, Vol. 6, 6, pp. 2294-2300.

74. **Otsuka, M., Matsuda, Y., Suwa, Y., Fox, J. L., Higuchi, W. I.** A novel skeletal drug delivery system using self-setting calcium phosphate cement. 2. Physicochemical properties and drug release rate of the cement-containing indomethacin. *Journal of pharmaceutical sciences.* 1994, Vol. 83, 5, pp. 611-615.

75. **Durucan, C., Brown, P.W.** α-Tricalcium phosphate hydrolysis to hydroxyapatite at and near physiological temperature. *Journal of materials science: Materials in medicine.* 2000, Vol. 11, 6, pp. 365-371.

76. **Morejón-Alonso, L., Ferreira, O. J. B., Carrodeguas, R. G., dos Santos, L. A.** Bioactive composite bone cement based on α-tricalcium phopshate/tricalcium silicate. *Journal of biomedical materials research part B: Applied biomaterials.* 2011, Vol. 100B, 1, pp. 94-102.

77. **Sugo, K., Kawashima, R., Nakasu, M., Nakajima, T.** Antibiotic elution profile and physical properties of a novel calcium phosphate cement material. *Journal of the ceramic society of Japan.* 2016, Vol. 124, 9, pp. 954-958.

78. **Noukrati, H., Cazalbou, S., Demnati, I., Rey, C., Barroug, A., Combes, C.** Injectability, microstructure and release properties of sodium fusidate-loaded apatitic cement as a local drug-delivery system. *Materials science and engineering: C.* 2016, Vol. 59, pp. 177-184.

79. **Ginebra, M. P., Traykova, T., Planell, J. A.** Calcium phosphate cements as bone drug delivery systems: A review. *Journal of controlled release.* 2006, Vol. 113, pp. 102-110.

80. **Ritger, P. L., Peppas, N. A.** A simple equation for description of solute release I. Fickian and non-fickian elease from non-swellable devices in form of slabs, spheres, cylinders or discs. *Journal of controlled release.* 1987, Vol. 5, 1, pp. 23-36.

81. **Brunner, T. J.** Application of nanoparticulate biomaterials for injectable bone cements and dental repair. 2007.

82. **Andrews, D. L.** Rayleigh scattering and Raman effect, Theory. [book auth.] Tranter G. E., Koppenaal D. W. Lindon J. C. *Encyclopedia of spectroscopy and spectrometry.* 2nd. s.l. : Elsevier, Academic Press, 2010, pp. 2413-2419.